https://doi.org/10.1016/j.energy.2017.12.065

A new algorithm for obtaining the critical tube diameter and intercept factor of parabolic trough solar collectors

Bin Zou[1, 2], Yang Yao[1], Yiqiang Jiang[1*], Hongxing Yang[2]

[1] Department of Building Thermal Energy Engineering, Harbin Institute of Technology, Harbin, China

[2] Renewable Energy Research Group (RERG), Department of Building Services Engineering, The Hong Kong Polytechnic University, Hong Kong, China

Abstract

A new algorithm for obtaining the critical tube diameter and intercept factor of parabolic trough solar collectors (PTCs) under the condition of tube alignment error has been developed theoretically, which, compared with the Monte Carlo Ray Tracing (MCRT) method, reduces the computing time remarkably. The results produced by the proposed method comply very well with the results obtained by MCRT. The critical tube diameters for different alignment errors can be precisely calculated using the algorithm, which can also be used to explain well the variation of optical efficiency. Effects of structural parameters on the optical performance are also discussed comprehensively. It is revealed that the offset direction that is perpendicular to the focus-edge connection line is most likely to cause rays-escaping. There exists an aperture width range (and also focal length range) in which the optical efficiency decreases with increasing offset angle, which is contrary to the conclusion presented in previous literature that the effects of X-direction offset (a=0°) is greater than that in Y-direction (a=90°). The proposed algorithm establishes the foundation for further geometric study on the coupling effects of multi-errors on PTCs' performance, and can also be used for quick calculation and analysis in practice.

Keywords: Parabolic trough solar collector; Algorithm; Critical tube diameter; Intercept factor; Optical efficiency; Tube alignment error.

* Corresponding author: Department of Building Thermal Energy Engineering, Harbin Institute of Technology, Harbin, China

Tel. / fax: +86-451-86282123 E-mail address: jyq7245@sina.com (Y. Jiang)

Nomenclature

a	offset angle (°)	η_o	optical efficiency (%)
d_a	absorber tube outer diameter (m)	$\Delta\eta_o$	optical efficiency difference between the proposed method and MCRT (%)
d_g	glass envelope outer diameter (m)	θ	radial angular displacement of line source (rad)
$d_{\min}$	critical tube diameter in ideal condition (m)	θ_{in}	incident angle (rad)
$d_{re,a}$	critical tube diameter in tube alignment error condition (m)	θ'	radial angle of any point in the light cone (rad)
e	angle for auxiliary calculation (°)	$\Delta\theta$	angle span in which the absorber tube receives sunrays (°)
f	focal length (m)	φ_s	circumferential angle of the point on the solar disk (rad)
l	the height of light cone (m)	ρ_r	reflectivity of the parabolic reflector
l_a	offset distance (m)	τ_g	transmissivity of the glass envelope
l_{shade}	length of the shaded part of the reflector by absorber tube (m)	ψ	position angle of the point on the parabolic reflector (°)
W	aperture width (m)	ψ_{rim}	rim angle (°)
Greek symbols		***Abbreviations***	
α_a	absorptivity of the absorber	CSC	concentrating solar collector
β	angle in the light cone corresponding to the actual absorber tube radius (rad)	CSP	concentrating solar power
β'	angle in the light cone corresponding to the critical radius (rad)	FVM	Finite Volume Method

γ	intercept factor	HTF	heat transfer fluid
γ_{shade}	intercept factor for the shaded part of the reflector by absorber tube	MCRT	Monte Carlo Ray Tracing
δ	radial angle of the sun (δ =4.65mrad)	PTC	parabolic trough solar collector

1. Introduction

Exploitation and utilization of renewable energy, especially solar energy, is a promising alternative solution to relieve the severe environmental and energy issues [1-3], which has attracted extensive attentions [4, 5]. The parabolic trough solar collector (PTC) technology is the most cost-effective and mature technology for utilization of solar energy in concentrating solar power (CSP) area [6-8]. It has also been applied in many other fields, such as industrial process heat production, desalination, drying, refrigeration and air-conditioning [9-14], showing great development prospects.

Incident solar rays are reflected by the parabolic reflector onto the receiver tube that is installed along the focal line, and then absorbed and converted to thermal energy, and transferred to the heat transfer fluid (HTF) flowing in the absorber tube. Thus, a good rays-concentrating process is of great significance to ensure a high performance for the PTC. There are numerous studies conducted on the optical performance of PTCs. During 1970s and 1980s, researchers [15-20] developed optical cone method combined with geometrical analysis for investigating PTCs' optical performance, and found some basic properties. Grena [21, 22] developed a three-dimensional model based on the ray tracing recursive algorithm and further discussed the efficiency gain with an infrared-reflective film on the non-radiation part of the receiver. Khanna et al. [23] developed analytical expressions for both the circumferential and axial flux distribution on a bent absorber tube. Later, they validated their optical models using experimental results [24]. In recent years, with the development of computer technologies, the Monte Carlo Ray Tracing (MCRT) method has been widely used to study the optical characteristics of concentrating solar collectors (CSC) [25-28]. MCRT has high accuracy and flexibility. However, it has large computational complexity, needing long computing time and hence causing inconvenience for engineering application. Cheng et al. [29-31] developed a unified MCRT code for typical concentrating solar collectors (CSC) and investigated the optical performance of different PTCs based on the developed code. In their studies, a very important conclusion was drawn that the rays-escaping effect weakens the optical efficiency dramatically. Liang et al. [32] compared three optical models and presented that the model that uses Finite Volume Method (FVM) to determine photons distribution and changes photon energy by multiplying reflectivity, transmissivity and absorptivity has the shortest computing time. Guo et al. [33] discussed the influences of various operational conditions in terms of both heat loss and exergy loss. They argued that optical heat loss far outweighed the heat loss of receiver. Therefore, the high-quality of concentrating rays, which is usually represented by high optical efficiency, is the basis to achieve a high operational performance for the PTC system.

Because of the finite size of solar disk, the solar beam are not parallel (light cone), forming a focal shape on the surface of the absorber tube after reflection. If the size of the focal shape is larger than the absorber tube diameter, rays will escape from around the tube, causing huge optical loss. This rays-escaping effect has been discussed in previous studies [30, 34] which proposed that the absorber tube diameter should be larger than the critical tube diameter to avoid rays-escaping. The critical tube diameter is the required minimum tube diameter that can receive all the reflected rays. The theoretical formulas for calculating critical diameter in both ideal and tracking error conditions were derived in previous literature [30, 32]. However, the critical diameter under the condition of tube alignment error has never been given. The widely used MCRT can just provide an approximation of the true critical diameter and cannot be used to analyze the variation of critical diameter with different optical errors and structural parameters. In addition, the MCRT has great computational complexity, needing long computing time, which is very inconvenient to be used for engineering calculation and analysis. This paper derives theoretically the formulas of critical diameter under the condition of tube alignment error. Based on the derived formulas, a simple algorithm for obtaining the intercept factor (or optical efficiency) is further developed, which, compared with MCRT, can reduce the computing time remarkably from hours to seconds. The results obtained by the proposed methods are consistent with that obtained by MRCT, verifying the accuracy and reliability of the developed algorithm. The changing properties of the optical efficiency can be explained well by the derived critical diameter, which further proves mutually the accuracy of each other. The current work in this paper is the foundation of detailed geometric analysis which is what we are going to do in the next study on the coupling effects of multi-errors, such as tracking error, surface error, installation error and practical sun-shape, on PTC's performance. It is also an effective method that can be used to do quick calculation and analysis in engineering practice.

2. Physical model and algorithm description

2.1 Physical model

As Fig. 1 shows, a parabolic trough solar collector (PTC) is made up of a parabolic reflector and a receiver tube which consists mainly of a metal absorber tube with selective absorbing coatings on its outer surface and a glass envelope. The annulus between the metal absorber and glass envelope is kept vacuum to reduce heat loss and protect the coatings from oxidation. Several important parameters, including aperture width (W), focal length (f), absorber tube outer diameter (d_a), glass envelope diameter (d_g), rim angle (ψ_{rim}), and radial angle of the sun (δ signifies the finite size of the solar disk) are shown in the figure as well. A Cartesian coordinate system OXYZ used in this paper is also established.

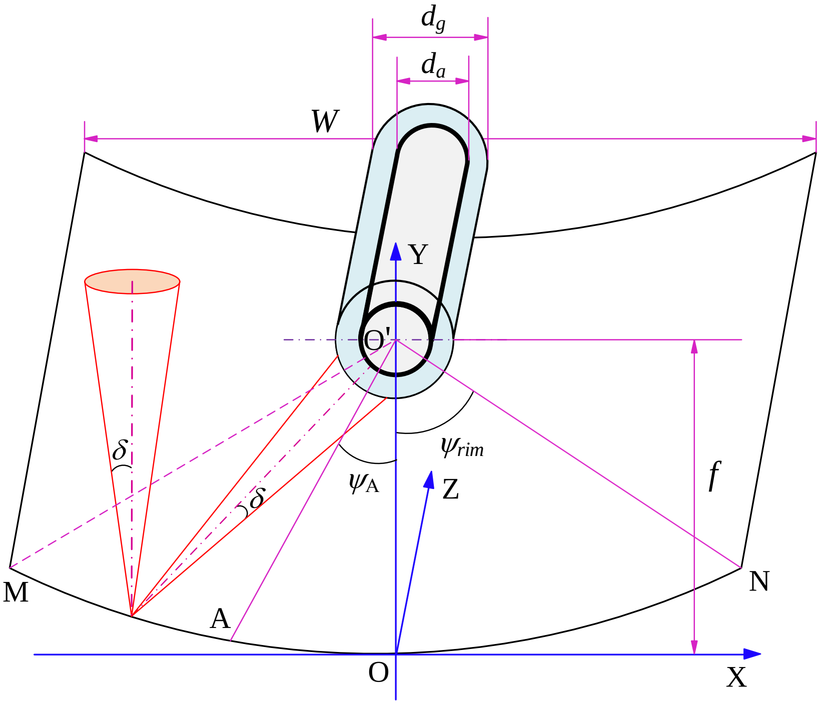

Fig. 1 Schematic of a PTC module

The SEGS LS-2 PTC module has been tested on the AZTRAK rotating test platform at Sandia National Laboratory (SNL), and detailed test data were collected [35]. In this study, the SEGS LS-2 PTC module is also used as the physical prototype for analysis, the major parameters of which are listed in Table 1.

Table 1 Parameters of SEGS LS-2 PTC module

Parameter	Value	Unit
W	5	m
f	1.84	m
L_a	7.8	m
d_a	0.07	m
d_g	0.115	m
α_a	0.96	——
ρ_r	0.93	——

τ_g	0.95	——

2.2 Critical tube diameter

As mentioned above, the critical tube diameter is the required minimum diameter to avoid rays escaping which affects the optical performance of a PTC significantly. For ideal conditions (without any optical errors), the critical tube diameter for any point A (as shown in Fig. 1) on the parabolic reflector has been proposed in Refs. [30, 31], which is expressed by Eq. (1).

$$d_{\min} = 2 \cdot \left(\frac{x_{\mathrm{A}}^2}{4f} + f \right) \cdot \sin \delta \tag{1}$$

where x_{A} is the abscissa of point A. The position angle (ψ_{A}) for point A is the angle between line $\overline{\mathrm{AO'}}$ and Y-axis, theoretically given by Eq. (2).

$$\psi_{\mathrm{A}} = \begin{cases} \arcsin\left(\dfrac{|x_{\mathrm{A}}|}{x_{\mathrm{A}}^2 / 4f + f} \right) & 0^{\circ} < \psi_{\mathrm{A}} \le 90^{\circ} \\ 180^{\circ} - \arcsin\left(\dfrac{|x_{\mathrm{A}}|}{x_{\mathrm{A}}^2 / 4f + f} \right) & 90^{\circ} < \psi_{\mathrm{A}} < 180^{\circ} \end{cases} \tag{2}$$

where $|x_{\mathrm{A}}|$ is the absolute value of the abscissa of point A. As Fig. 2 shows, point A is any point on the left half of the parabolic reflector ($x_{\mathrm{A}} \le 0$) and line $\overline{\mathrm{AO'}}$ is the centerline of the reflected light cone. For simplicity, we define the clockwise direction as the right side of vector $\overrightarrow{\mathrm{AO'}}$. In Fig. 2, point $\mathrm{O'}$ is the focus of the parabola, and the absorber tube is installed away from the focus with an offset distance (l_a) and an offset angle (a). The outermost rays of the reflected light cone are tangent to the dotted circle. Thus the diameter of the dotted circle is the critical diameter.

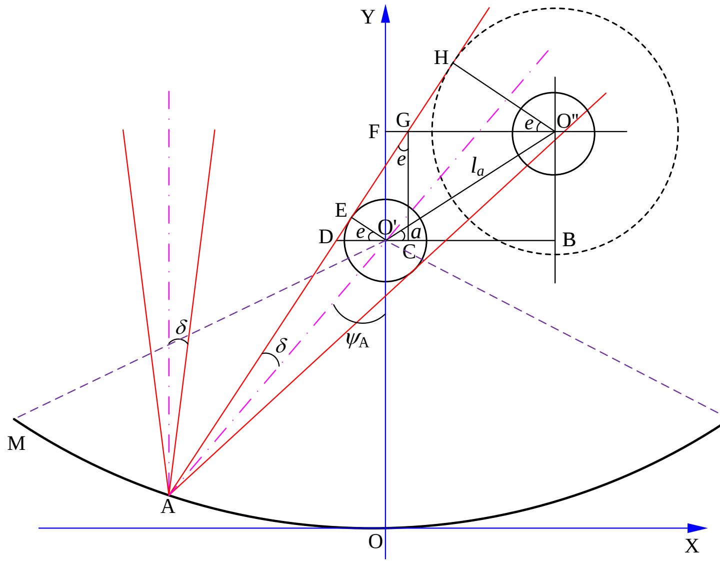
Y
H
G
F
O''
e
l_a
E
D
O'
a
C
B
δ
ψ_A
M
N
A
O
X

(a)

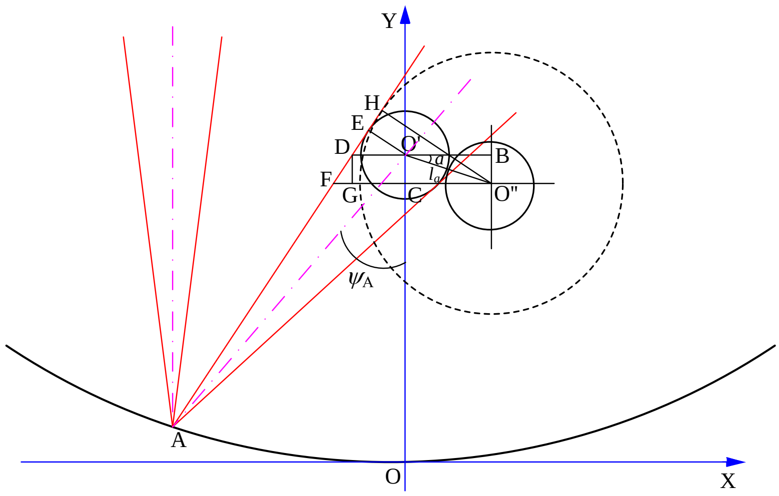
Y
H
E
D
O'
a
B
F
l_a
G
C
O''
ψ_A
A
O
X

(b)

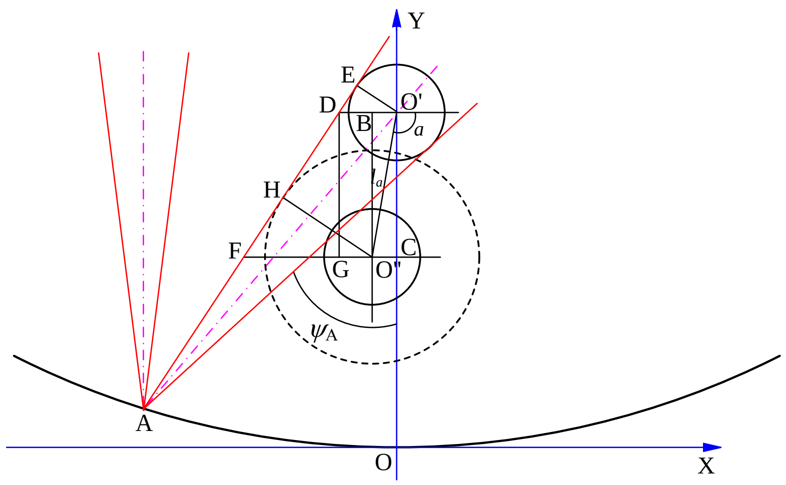
Y
E
D
O'
B
a
l_a
H
F
G
O''
C
ψ_A
A
O
X

(c)

Fig. 2 Offset direction is on the right side of line $\overline{\mathrm{AO'}}$ for $0^{\circ} < \psi_{\mathrm{A}} \le 90^{\circ}$: (a) $0 < a \le 90 - \psi_{\mathrm{A}}$, (b) $-90 < a \le 0$, (c) $-90 - \psi_{\mathrm{A}} < a \le -90$

For $0^{\circ} < \psi_{\mathrm{A}} \le 90^{\circ}$, when the offset direction is on the right side of line $\overline{\mathrm{AO'}}$ ($-90^{\circ} - \psi_{\mathrm{A}} < a \le 90^{\circ} - \psi_{\mathrm{A}}$), it can be divided into three cases, which are $0 < a \le 90^{\circ} - \psi_{\mathrm{A}}$, $-90^{\circ} < a \le 0$ and $-90^{\circ} - \psi_{\mathrm{A}} < a \le -90^{\circ}$ (as shown in Fig. 2(a), Fig. 2(b), Fig. 2(c) respectively). Taking the case of $0 < a \le 90^{\circ} - \psi_{\mathrm{A}}$ (as shown in Fig. 2(a)) as an example, we present the detailed derivation process of the critical tube diameter ($d_{re,a}$), which is given as follow.

Easily, in Fig. 2(a), the auxiliary calculation angle (e) can be given by Eq. (3).

$$e = \psi_{\mathrm{A}} - \delta \tag{3}$$

The derivation process of critical tube diameter ($d_{re,a}$) is given as follow:

$$\begin{aligned}
d_{re,a} &= 2\times \mathrm{O''H} = 2\times \mathrm{O''G}\times\cos(e) = 2\times(\mathrm{O''F}-\mathrm{GF})\times\cos(e) \\
&= 2\times(\mathrm{BO'}-\mathrm{CO'})\times\cos(e) = 2\times\left[\mathrm{BO'}-(\mathrm{CD}-\mathrm{O'D})\right]\times\cos(e) \\
&= 2\times\left[\left|\mathrm{O'O''}\times\cos(a)\right| - \mathrm{GC}\times\tan(e) + \frac{\mathrm{EO'}}{\cos(e)}\right]\times\cos(e) \\
&= 2\times\left[\left|\mathrm{O'O''}\times\cos(a)\right| - \mathrm{O''B}\times\tan(e) + \frac{\mathrm{EO'}}{\cos(e)}\right]\times\cos(e) \\
&= 2\times\left[l_a\times\cos(a) - l_a\times\sin(a)\times\tan(e) + \frac{d_{\min}}{2\times\cos(e)}\right]\times\cos(e) \\
&= 2\times\left[l_a\times\cos(a)\cos(e) - l_a\times\sin(a)\times\sin(e) + \frac{d_{\min}}{2}\right] \\
&= 2\times l_a\times\cos(a+e) + d_{\min}
\end{aligned}$$

Combined with Eq. (3), $d_{re,a}$ can be expressed by Eq. (4).

$$d_{re,a}=2\times l_a \times \cos\left(a+\psi_{\mathrm{A}}-\delta\right)+d_{\min} \tag{4}$$

Similarly, we can derive the expressions of $d_{re,a}$ for the other two cases ($-90^{\circ}<a\leq 0$ and $-90^{\circ}-\psi_{\mathrm{A}}<a\leq -90^{\circ}$), which actually are the same as Eq. (4). Therefore, when the offset direction is on the right side of line $\overline{\mathrm{AO'}}$ ($-90^{\circ}-\psi_{\mathrm{A}}<a\leq 90^{\circ}-\psi_{\mathrm{A}}$), the mathematical expression of $d_{re,a}$ is given by Eq. (5).

$$d_{re,a}=2\times l_a \times \cos\left(a+\psi_{\mathrm{A}}-\delta\right)+d_{\min} \qquad -90^{\circ}-\psi_{\mathrm{A}}<a\leq 90^{\circ}-\psi_{\mathrm{A}} \tag{5}$$

When the offset direction is on the left side of line $\overline{\mathrm{AO'}}$ ($90^{\circ}-\psi_{\mathrm{A}}<a\leq 270^{\circ}-\psi_{\mathrm{A}}$), it can also be divided into three cases, which are $90^{\circ}-\psi_{\mathrm{A}}<a\leq 90^{\circ}$, $90^{\circ}<a\leq 180^{\circ}$ and $180^{\circ}<a\leq 270^{\circ}-\psi_{\mathrm{A}}$ (as shown in Fig. 3(a), Fig. 3(b), Fig. 3(c) respectively). Taking the case of $90^{\circ}-\psi_{\mathrm{A}}<a\leq 90^{\circ}$ (as shown in Fig. 3(a)) as an example, we give the detailed derivation of $d_{re,a}$.

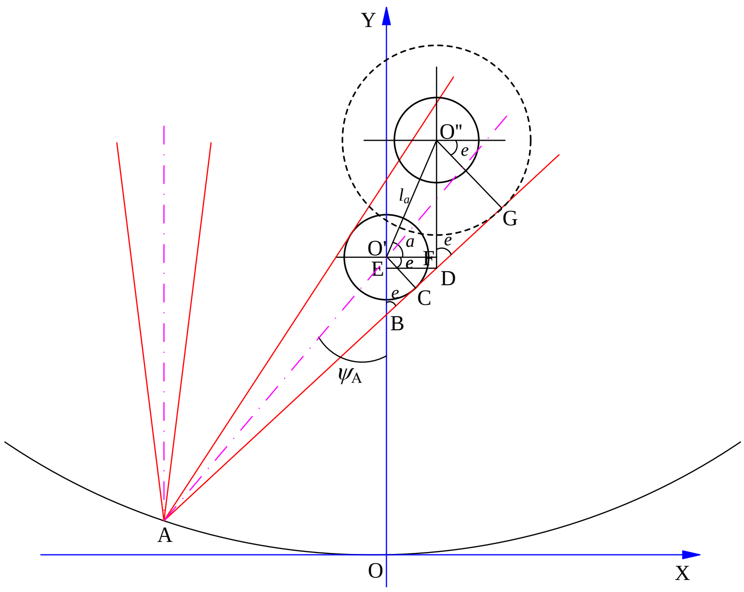

(a)

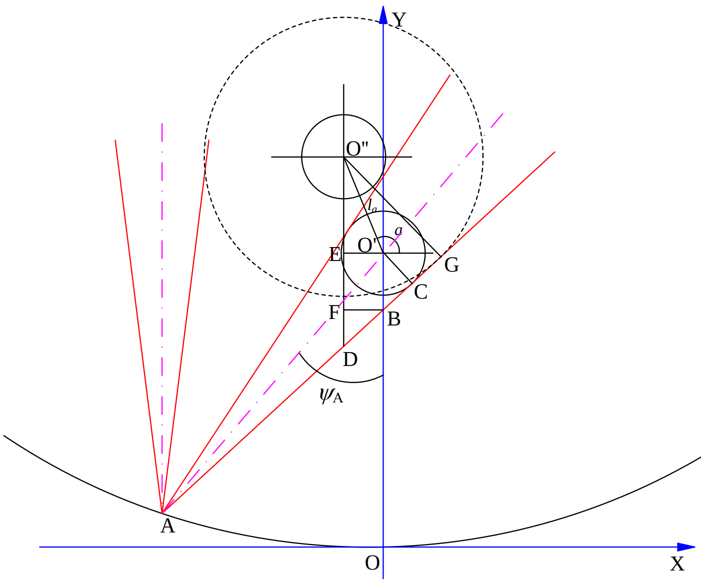

(b)

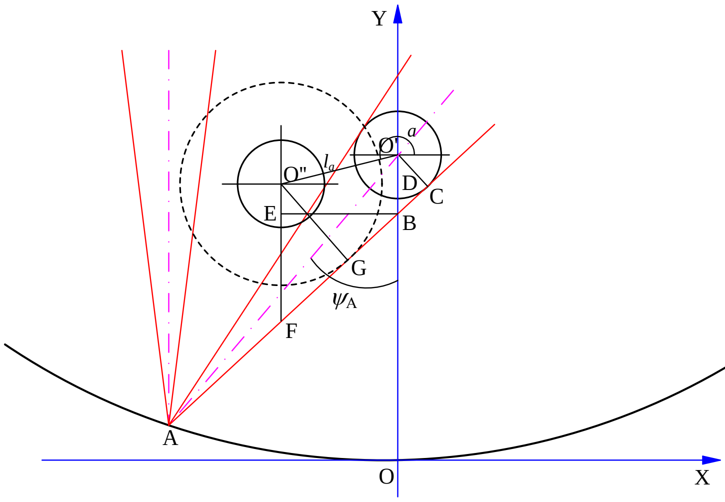

(c)

Fig. 3 Offset direction is on the left side of line $\overline{AO'}$ for $0^o < \psi_A \le 90^o$: (a) $90 - \psi_A < a \le 90$, (b) $90 < a \le 180$, (c) $180 < a \le 270 - \psi_A$

Obviously, the auxiliary calculation angle (e) in Fig. 3(a) can be given by Eq. (6).

$$e = \psi_A + \delta \tag{6}$$

The derivation process of critical tube diameter ($d_{re,a}$) is given as follow:

$$d_{re,a} = 2\times \mathrm{O''G} = 2\times \mathrm{O''D}\times\sin(e) = 2\times(\mathrm{O''F}+\mathrm{FD})\times\sin(e)$$

$$= 2\times(\mathrm{O''F}+\mathrm{O'E})\times\sin(e) = 2\times[\mathrm{O''F}+\mathrm{O'B}-\mathrm{EB}]\times\sin(e)$$

$$= 2\times\left[\left|\mathrm{O'O''}\times\sin(a)\right| + \frac{\mathrm{O'C}}{\sin(e)} - \mathrm{ED}\times\cot(e)\right]\times\sin(e)$$

$$= 2\times\left[\mathrm{O'O''}\times\sin(a) + \frac{\mathrm{O'C}}{\sin(e)} - \mathrm{O'F}\times\cot(e)\right]\times\sin(e)$$

$$= 2\times\left[l_a\times\sin(a) + \frac{d_{\min}}{2\times\cos(e)} - \left|l_a\times\cos(a)\right|\times\cot(e)\right]\times\sin(e)$$

$$= 2\times\left[l_a\times\sin(a)\times\sin(e) - l_a\times\cos(a)\cos(e) + \frac{d_{\min}}{2}\right]$$

$$= -2\times l_a\times\cos(a+e) + d_{\min}$$

Combined with Eq. (6), $d_{re,a}$ can be expressed by Eq. (7).

$$d_{re,a} = -2\times l_a\times\cos(a+\psi_{\mathrm{A}}+\delta) + d_{\min} \tag{7}$$

The expressions of $d_{re,a}$ for the other two cases ($90^{\circ} < a \leq 180^{\circ}$ and $180^{\circ} < a \leq 270^{\circ} - \psi_{\mathrm{A}}$) can also be obtained by the same way, which actually are the same as Eq. (7). Therefore, when the offset direction is on the left side of line $\overline{\mathrm{AO'}}$ ($90^{\circ} - \psi_{\mathrm{A}} < a \leq 270^{\circ} - \psi_{\mathrm{A}}$), the mathematical expression of $d_{re,a}$ is given by Eq. (8).

$$d_{re,a} = -2\times l_a\times\cos(a+\psi_{\mathrm{A}}+\delta) + d_{\min} \qquad 90^{\circ} - \psi_{\mathrm{A}} < a \leq 270^{\circ} - \psi_{\mathrm{A}} \tag{8}$$

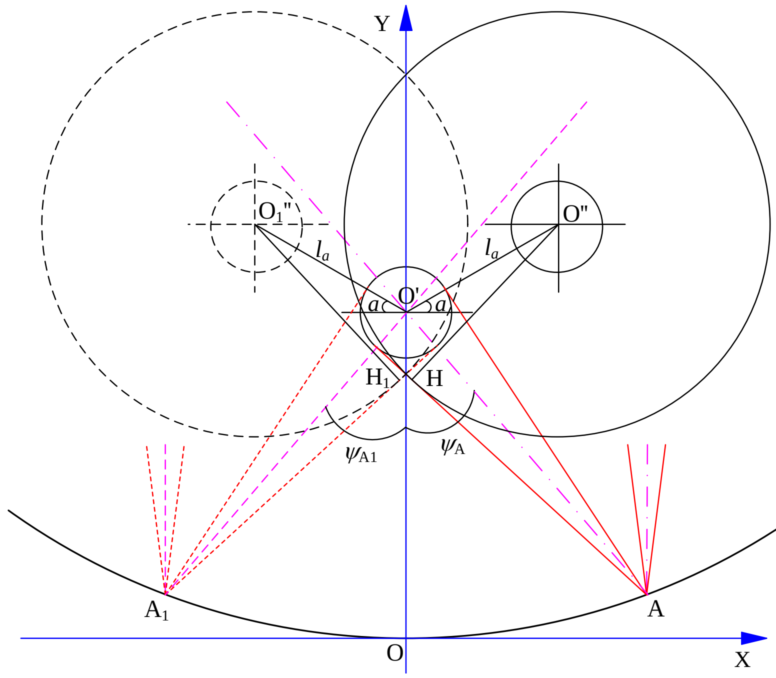

Fig. 4 The situation that point A is on the right half of the reflector ($x_{\mathrm{A}} > 0$)

When point A is on the right half of the parabolic reflector ($x_{\mathrm{A}} > 0$), the critical tube diameter ($d_{re,a}$) can be obtained similarly due to the symmetry of parabola. Fig. 4 shows the situation that point A is on the right half the parabolic reflector ($x_{\mathrm{A}} > 0$). Obviously, the critical diameter ($d_{re,a}$) is equal to twice $\overline{\mathrm{O''H}}$ ($d_{re,a} = 2\times\overline{\mathrm{O''H}}$). Point A₁ and point A are symmetrical about Y-axis. From the figure, it can be clearly seen that $\overline{\mathrm{O''H}}$ is equal to $\overline{\mathrm{O_1''H_1}}$ ($\overline{\mathrm{O''H}} = \overline{\mathrm{O_1''H_1}}$). Therefore, the critical diameter ($d_{re,a}$) corresponding to a for $x_{\mathrm{A}} > 0$ is equal to the critical diameter corresponding to $180^{\circ} - a$ for $x_{\mathrm{A}} < 0$. Thus, using $180^{\circ} - a$ replacing a in Eq. (5) and Eq. (8), we can obtain the critical diameter ($d_{re,a}$) for $x_{\mathrm{A}} > 0$, which is presented as follow:

When the offset direction is on the right side of line $\overline{\mathrm{AO'}}$ ($\psi_{\mathrm{A}} - 90^{\circ} < a \le 90^{\circ} + \psi_{\mathrm{A}}$), the range of $180^{\circ} - a$ is $90^{\circ} - \psi_{\mathrm{A}} \le 180^{\circ} - a < 270^{\circ} - \psi_{\mathrm{A}}$, satisfying the condition of Eq. (8). Thus, $d_{re,a}$ can be calculated by Eq. (9).

$$d_{re,a} = -2\times l_a \times \cos\left(180^{\circ} - a + \psi_{\mathrm{A}} + \delta\right) + d_{\min} = 2\times l_a \times \cos\left(a - \psi_{\mathrm{A}} - \delta\right) + d_{\min} \quad (9)$$

Similarly, when the offset direction is on the left side of line $\overline{\mathrm{AO'}}$, we can calculate $d_{re,a}$ using Eq. (5), which is expressed by Eq. (10).

$$d_{re,a} = 2\times l_a \times \cos\left(180^{\circ} - a + \psi_{\mathrm{A}} - \delta\right) + d_{\min} = -2\times l_a \times \cos\left(a - \psi_{\mathrm{A}} + \delta\right) + d_{\min} \quad (10)$$

Considering that the critical diameter ($d_{re,a}$) is the required diameter to avoid rays escaping, we should select the maximum among the calculated diameters of all points on the reflector as the critical diameter ($d_{re,a}$) of the PTC. Summarizing Eq. (5), Eq. (8), Eq. (9) and Eq. (10), we can obtain the complete calculation formula of the critical diameter for $0^{\circ} < \psi_{\mathrm{A}} \le 90^{\circ}$, which is given by Eq. (11).

$$d_{re,a1} = \begin{cases} \max\left[2\times l_a \cos\left(a + \psi_{\mathrm{A}} - \delta\right) + d_{\min},\ -2\times l_a \cos\left(a - \psi_{\mathrm{A}} + \delta\right) + d_{\min}\right] & -90^{\circ} - \psi_{\mathrm{A}} < a \le -90^{\circ} + \psi_{\mathrm{A}} \\ \max\left[2\times l_a \cos\left(a + \psi_{\mathrm{A}} - \delta\right) + d_{\min},\ 2\times l_a \cos\left(a - \psi_{\mathrm{A}} - \delta\right) + d_{\min}\right] & -90^{\circ} + \psi_{\mathrm{A}} < a \le 90^{\circ} - \psi_{\mathrm{A}} \\ \max\left[-2\times l_a \cos\left(a + \psi_{\mathrm{A}} + \delta\right) + d_{\min},\ 2\times l_a \cos\left(a - \psi_{\mathrm{A}} - \delta\right) + d_{\min}\right] & 90^{\circ} - \psi_{\mathrm{A}} < a \le 90^{\circ} + \psi_{\mathrm{A}} \\ \max\left[-2\times l_a \cos\left(a + \psi_{\mathrm{A}} + \delta\right) + d_{\min},\ -2\times l_a \cos\left(a - \psi_{\mathrm{A}} + \delta\right) + d_{\min}\right] & 90^{\circ} + \psi_{\mathrm{A}} < a \le 270^{\circ} - \psi_{\mathrm{A}} \end{cases} \quad (11)$$

where $d_{\min}$ and ψ_{A} are given by Eq. (1) and Eq. (2) respectively.

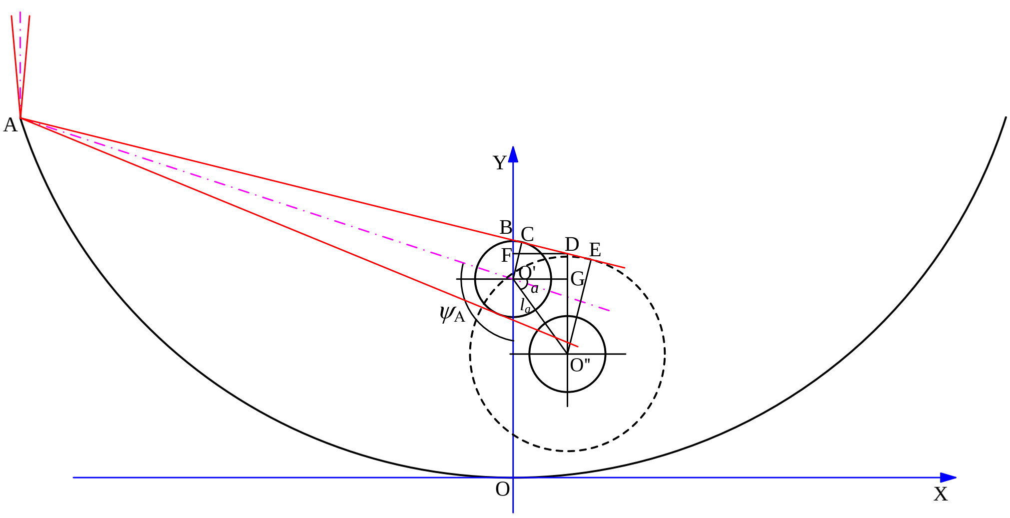

(a)

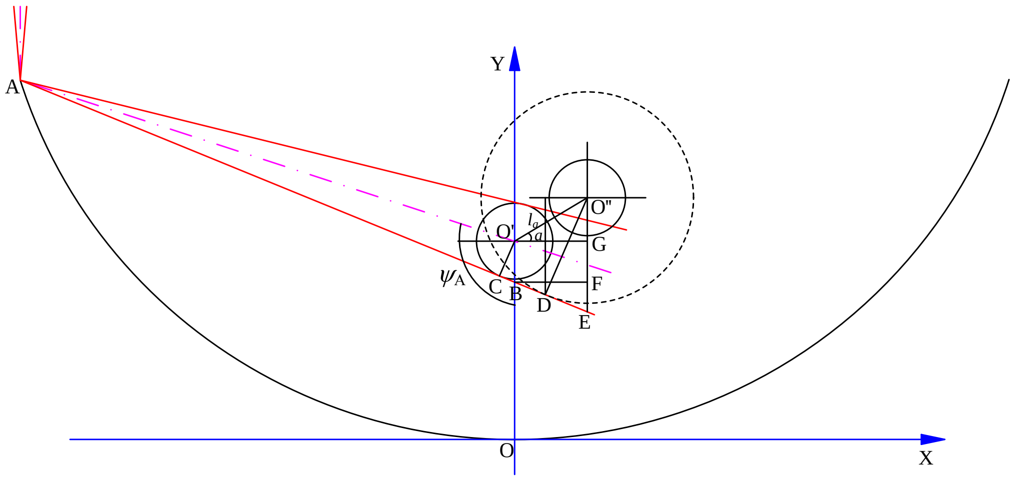

(b)

Fig. 5 The case of $90^{\circ} < \psi_{\mathrm{A}} < 180^{\circ}$: (a) offset direction is on the right side, (b) offset direction is on the left side

For $90^{\circ} < \psi_{\mathrm{A}} < 180^{\circ}$ (as shown in Fig. 5), the calculation formula of critical diameter can be derived by the same way, which is given by Eq. (12).

$$d_{re,a2} = \begin{cases} \max\left[2\times l_a\cos\left(a+\psi_{\mathrm{A}}-\delta\right)+d_{\min},\quad 2\times l_a\cos\left(a-\psi_{\mathrm{A}}-\delta\right)+d_{\min}\right] & -90^{\circ}-\psi_{\mathrm{A}} < a \le -270^{\circ}+\psi_{\mathrm{A}} \\ \max\left[2\times l_a\cos\left(a+\psi_{\mathrm{A}}-\delta\right)+d_{\min},\quad -2\times l_a\cos\left(a-\psi_{\mathrm{A}}+\delta\right)+d_{\min}\right] & -270^{\circ}+\psi_{\mathrm{A}} < a \le 90^{\circ}-\psi_{\mathrm{A}} \\ \max\left[-2\times l_a\cos\left(a+\psi_{\mathrm{A}}+\delta\right)+d_{\min},\quad -2\times l_a\cos\left(a-\psi_{\mathrm{A}}+\delta\right)+d_{\min}\right] & 90^{\circ}-\psi_{\mathrm{A}} < a \le -90^{\circ}+\psi_{\mathrm{A}} \\ \max\left[-2\times l_a\cos\left(a+\psi_{\mathrm{A}}+\delta\right)+d_{\min},\quad 2\times l_a\cos\left(a-\psi_{\mathrm{A}}-\delta\right)+d_{\min}\right] & -90^{\circ}+\psi_{\mathrm{A}} < a \le 270^{\circ}-\psi_{\mathrm{A}} \end{cases} \tag{12}$$

Therefore, the critical diameter ($d_{re,a}$) of the PTC is finally given by Eq. (13).

$$d_{re,a} = \max\left(d_{re,a1},\ d_{re,a2}\right) \qquad -0.5W < x_{\mathrm{A}} \le 0 \tag{13}$$

2.3 Intercept factor

Intercept factor (γ) is defined as the ratio of rays intercepted by the absorber to the total rays incident on the aperture of the reflector. It reflects directly the degree of receiving rays of the absorber. The larger the intercept factor is, the more the reflected rays will be received by the absorber tube, and thereby the higher the optical efficiency (η_o) will be. In this section, a new simple algorithm for obtaining intercept factor (γ) and optical efficiency (η_o) under condition of tube alignment error will be developed.

Fig. 6 shows the reflection process of sun rays. From the figure, it is clearly seen that the solar disk can be viewed as consisting of countless line light sources which are parallel to the axial direction (Z-axis direction) of the absorber. It can be easily understood that a line light source on the solar disk will also form a line light on the absorber tube after reflection. As a result, if we can obtain the intensity of the line light source, the sun-shape (brightness of the solar disk) can be expressed just by the radial angular displacement of line light source (θ), which will reduce the computational complexity significantly. The derivation of the intensity of the line light source is given as follow:

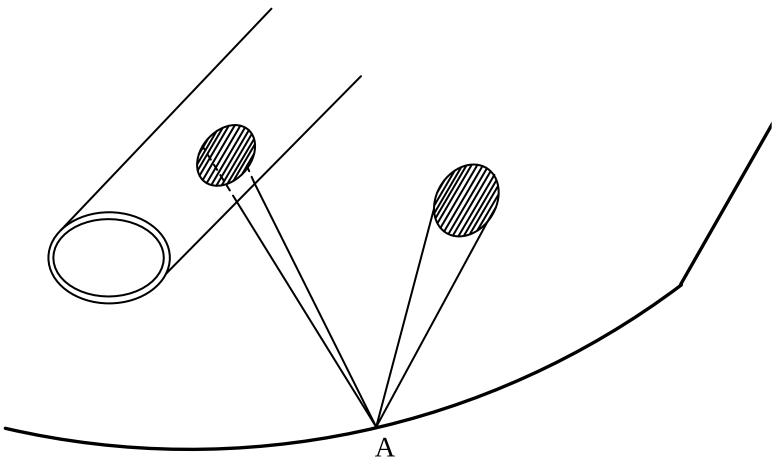

Fig. 6 The reflection process of sun rays

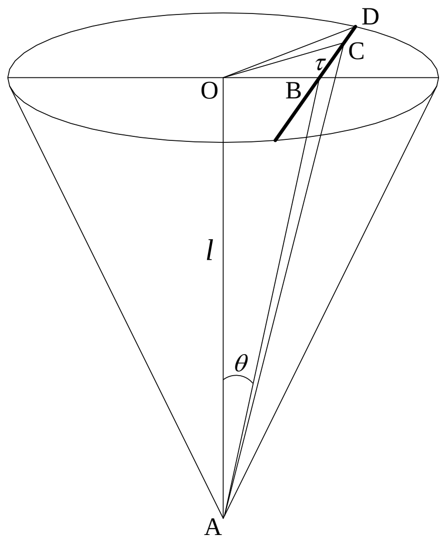

Fig. 7 Schematic of the light cone

Fig. 7 shows the schematic of the light cone. In the figure, AO=l, $\angle$BAO=θ, BC=τ. In $\triangle$AOB, OB can be calculated by Eq. (14):

$$\mathrm{OB}=\mathrm{AO}\times\tan\left(\theta\right)=l\times\tan\left(\theta\right) \tag{14}$$

In $\triangle$OBC, OC can be calculated by Eq. (15).

$$\mathrm{OC}=\sqrt{\mathrm{OB}^2+\mathrm{BC}^2}=\sqrt{\left(l\tan(\theta)\right)^2+\tau^2} \tag{15}$$

In $\triangle$AOC, $\angle$OAC can be calculated by Eq. (16).

$$\angle\mathrm{OAC}=\arctan\left(\frac{\mathrm{OC}}{\mathrm{OA}}\right)=\arctan\left(\frac{\sqrt{\left(l\tan(\theta)\right)^2+\tau^2}}{l}\right) \tag{16}$$

Assuming that the relative light intensity of any point on the sun disk is $\phi(\theta')$, we can calculate the intensity of the line light source, given by Eq. (17).

$$\psi(\theta)=2\times\int_{\mathrm{BD}}\phi\left[\arctan\left(\frac{\sqrt{\left(l\tan(\theta)\right)^2+\tau^2}}{l}\right)\right]d\tau=2\times\int_0^{\sqrt{\left(l\tan(\delta)\right)^2-\left(l\tan(\theta)\right)^2}}\phi\left[\arctan\left(\frac{\sqrt{\left(l\tan(\theta)\right)^2+\tau^2}}{l}\right)\right]d\tau \tag{17}$$

Make $\tau'=\dfrac{\tau}{l}$, Eq. (17) will be transformed to Eq. (18).

$$\psi(\theta) = 2l \times \int_0^{\sqrt{(\tan(\delta))^2 - (\tan(\theta))^2}} \phi\left[\arctan\left(\sqrt{(\tan(\theta))^2 + \tau'^2}\right)\right] d\tau' \qquad (18)$$

Given that the radial angle of the sun disk is very small (δ =0.00465rad), following formulas can be obtained:

$$\tan(\theta) = \theta, \qquad \tan(\delta) = \delta$$

Consequently, Eq. (18) will be simplified to Eq. (19).

$$\psi(\theta) = 2l \times \int_0^{\sqrt{\delta^2 - \theta^2}} \phi\left(\sqrt{\theta^2 + \tau'^2}\right) d\tau' \qquad (19)$$

Therefore, for any angle span ($\Delta\theta$) in the light cone, the total energy can be calculated by Eq. (20).

$$\Phi(\Delta\theta) = \int_{\Delta\theta} \psi(\theta)\, d\theta \qquad (20)$$

There are totally six cases of light concentration in the condition of tube alignment error, which are shown in Fig. 8(a) ~ Fig. 8(f) respectively. These six cases are listed as follows:

Case 1: The absorber cannot receive any rays;

Case 2: The absorber receives all rays;

Case 3: Partial rays escape from both sides of the absorber and the centerline of light cone does not cross the absorber;

Case 4: Partial rays escape from both sides of the absorber and the centerline of light cone crosses the absorber;

Case 5: Partial rays escape from one side of the absorber and the centerline of light cone does not cross the absorber;

Case 6: Partial rays escape from one side of the absorber and the centerline of light cone crosses the absorber.

To obtain the received energy for each case, we should first calculate several auxiliary parameters. As Fig. 8(a) shows, $\angle$EAO" (β) and $\angle$BAO" (β') are the angles in the light cone corresponding to the actual absorber tube radius ($0.5d_a$) and the critical radius ($0.5d_{re,a}$) respectively. Obviously, β and β' can be calculated by Eq. (21) and Eq. (22) respectively.

$$\beta = \arcsin\left(\frac{d_a}{2\times|\mathrm{AO}''|}\right) \tag{21}$$

$$\beta' = \arcsin\left(\frac{d_{re,a}}{2\times|\mathrm{AO}''|}\right) \tag{22}$$

The coordinates of point A and point O" are (x_{A} , $\frac{x_{\mathrm{A}}^2}{4f}$) and ($l_a\cos(a)$, $l_a\sin(a)+f$), respectively.

$$|\mathrm{AO}''| = \sqrt{\left(x_{\mathrm{A}} - l_a\cos(a)\right)^2 + \left(\frac{x_{\mathrm{A}}^2}{4f} - l_a\sin(a) - f\right)^2} \tag{23}$$

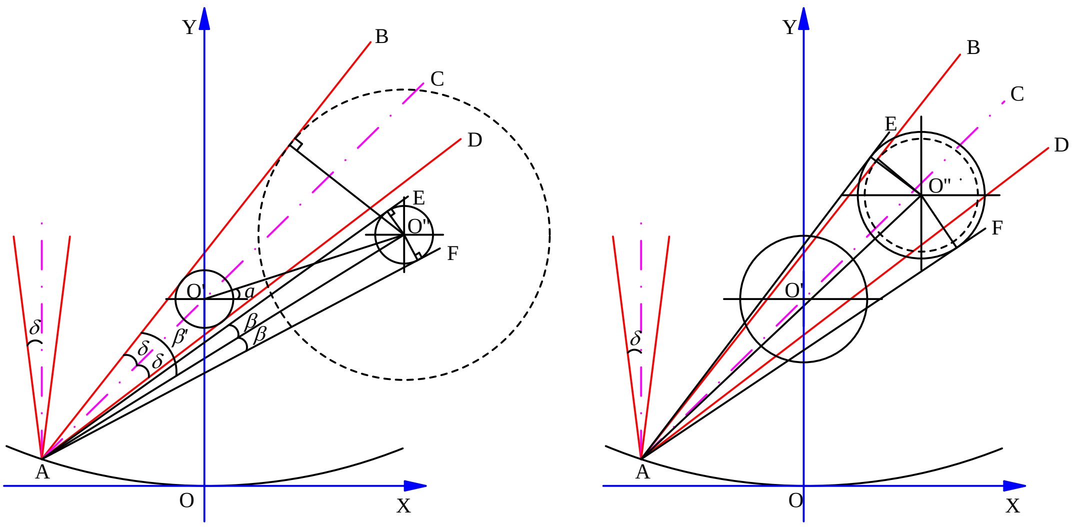

(a) (b)

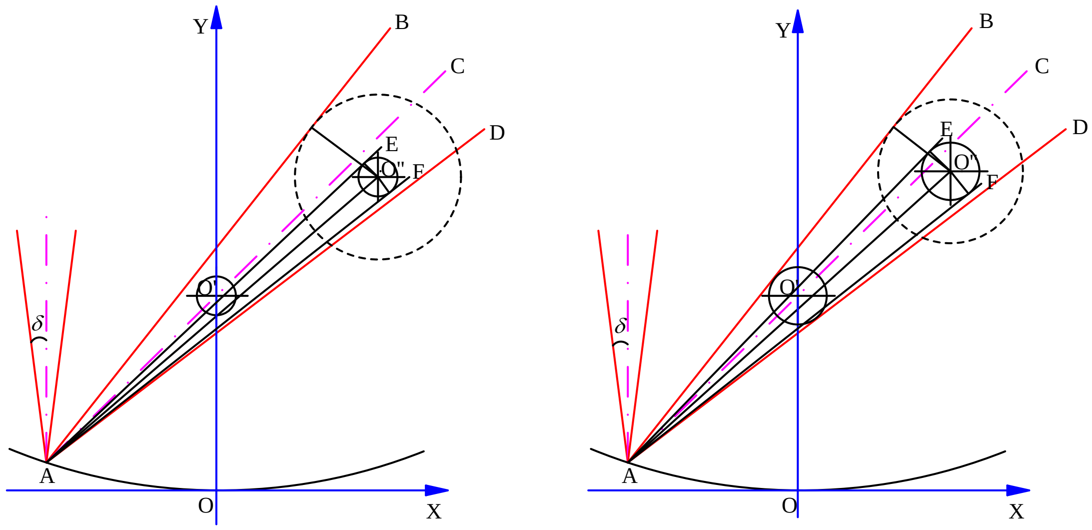

(c) (d)

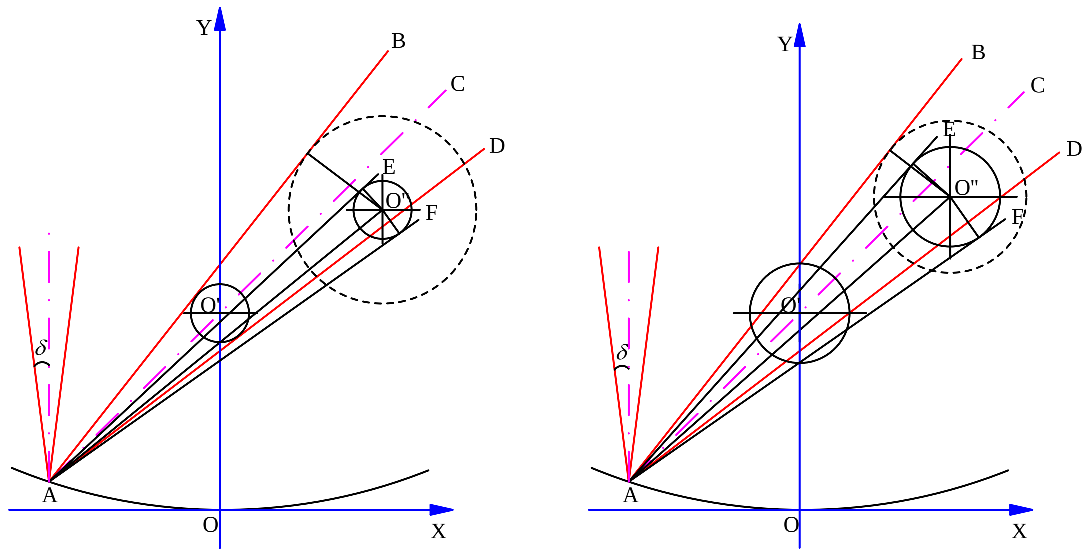

(e) (f)

Fig. 8 Different cases for light concentration in the condition of tube alignment error: (a) case 1, (b) case 2, (c) case 3, (d) case 4, (e) case 5, (f) case 6

From Fig. 8(a) to Fig. 8(f), the required conditions that β and β' should satisfy for each case can be easily obtained, which are listed in Table 2. The energy received by the absorber for each case can correspondingly be calculated by using Eq.

(20). The calculation formulas are also listed in Table 2.

Table 2 Required conditions and calculation formulas of received energy for each case

Cases	Required conditions	Calculation formulas
Case 1	$\beta'-\beta>2\delta$	$\Phi=0$
Case 2	$\beta'-\beta\le 0,\beta'+\beta\ge 2\delta$	$\Phi=2\times\int_0^{\delta}\psi(\theta)d\theta$
Case 3	$\beta'-\beta>\delta,\beta'+\beta\le 2\delta$	$\Phi=\int_{\beta'-\beta-\delta}^{\beta'+\beta-\delta}\psi(\theta)d\theta$
Case 4	$\beta'-\beta>0$, $\beta'-\beta\le\delta$, $\beta'+\beta\le 2\delta$	$\Phi=\int_0^{\beta'+\beta-\delta}\psi(\theta)d\theta+\int_0^{\delta-(\beta'-\beta)}\psi(\theta)d\theta$
Case 5	$\beta'-\beta>\delta$, $\beta'-\beta\le 2\delta$, $\beta'+\beta>2\delta$	$\Phi=\int_{\beta'-\beta-\delta}^{\delta}\psi(\theta)d\theta$
Case 6	$\beta'-\beta>0$, $\beta'-\beta\le\delta$, $\beta'+\beta>2\delta$	$\Phi=\int_0^{\delta-(\beta'-\beta)}\psi(\theta)d\theta+\int_0^{\delta}\psi(\theta)d\theta$

As a result, the total energy received by absorber for the whole reflector can be obtained by Eq. (24).

$$\mathrm{E}=\int_{-W/2}^{W/2}\Phi dx_{\mathrm{A}} \tag{24}$$

Thus, the intercept factor (γ) and the optical efficiency (η_o) can be given by Eq. (25) and Eq. (26) respectively.

$$\gamma=\frac{\mathrm{E}}{2\times\int_{-W/2}^{W/2}\int_0^{\delta}\psi(\theta)d\theta dx_{\mathrm{A}}} \tag{25}$$

$$\eta_o=\gamma\times\rho_r\times\tau_g\times\alpha_a\times 100\% \tag{26}$$

From Eq. (25) and Eq. (26), it can be easily seen that the intercept factor (γ) or the optical efficiency (η_o) is only related to W and $\Delta\theta$. Compared with MCRT which has to consider simultaneously W, z_{A}, θ' and φ_s, the computational complexity of the proposed algorithm is much smaller, reducing the computing time significantly. From Eq. (26), we can also know that the maximum optical efficiency will be obtained when the intercept factor is equal to 1 ($\gamma=1$), which is given by:

$$\eta_{o,\max} = 1\times 0.93\times 0.95\times 0.96\times 100\% = 84.816\%$$

3. Results and discussion

In this study, the brightness of solar disk is viewed as uniform, and the reflectivity, transmissivity and absorptivity are independent of the incident angle. The effects of refraction of the glass envelope are ignored. The incident angle is zero. The accuracy of the developed algorithm is first validated in the following part, and the optical performance under the condition of tube alignment error is then discussed comprehensively based on the proposed method.

3.1 Algorithm validation and effects of tube alignment error

Fig. 9 shows the variation of optical efficiency (η_o) with offset angle (a) for different offset distance (l_a). It can be seen from the figure that the results of the proposed method comply very well with that of MCRT, verifying the accuracy of the proposed algorithm. The results show that η_o varies significantly with a, and has different variation trends for different l_a. From the figure, it is also seen that the curve of η_o is almost symmetrical about a=0° for all l_a. When l_a is larger than

0.03m, η_o is smaller than the maximum (84.816%) for any a, indicating that rays escaping appears in this case. The reasons are shown in Fig. 10, which displays the variation of critical diameter ($d_{re,a}$) with offset angle (a) for different offset distance (l_a). From the figure, it can be seen that when l_a is more than 0.03m, $d_{re,a}$ is consistently larger than 0.07m which is the actual tube diameter for LS-2 PTC module (given in Table 1), causing rays escaping from around the absorber tube and consequently leading to optical loss. It can also be observed from Fig. 10 that when a is about 68.38° or -68.38°, $d_{re,a}$ is the maximum for any l_a. As given in Table 1, the rim angle of LS-2 PTC module is 68.38° ($\psi_{rim} = 68.38^{\circ}$). From Fig. 2(a), we can see that when a is 68.38° or -68.38°, the offset direction ($O'O''$) will be perpendicular to the connection line between focal point O' and edge point N or edge point M (defined as focus-edge connection line in this paper). Hence, it is concluded from above analyses that it is most likely to cause rays escaping effect in the case that the offset direction is perpendicular to the focus-edge connection line.

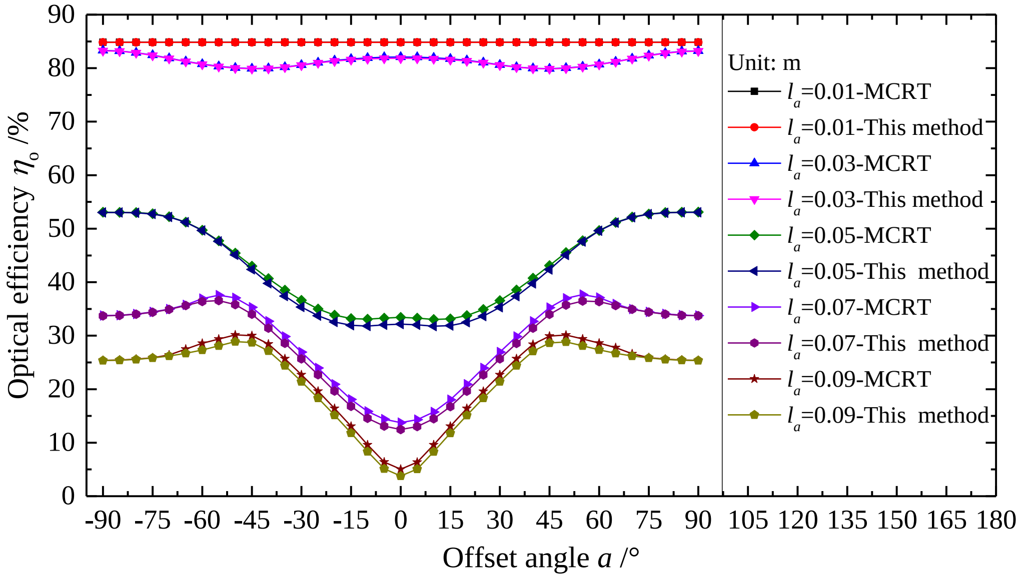

Fig. 9 Variation of optical efficiency (η_o) with offset angle (a) for different offset distance (l_a)

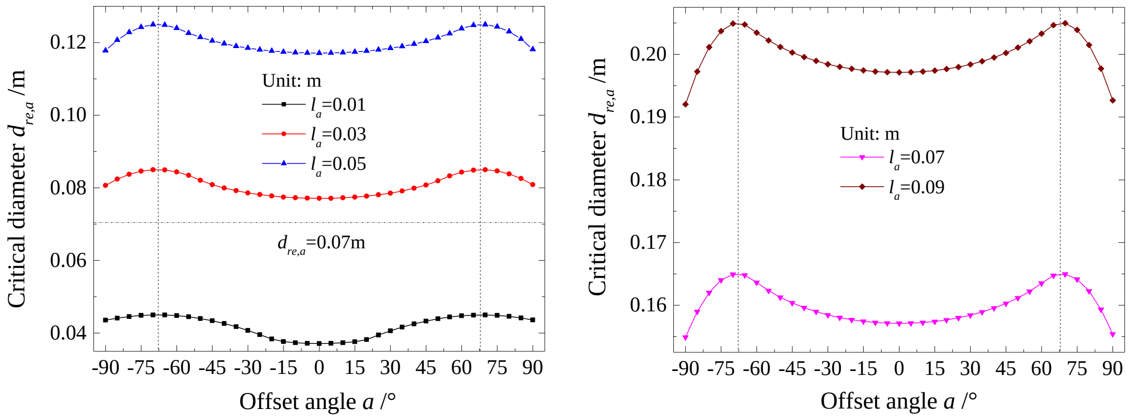

(a) (b)

Fig. 10 Variation of critical diameter ($d_{re,a}$) with offset angle (a) for different offset distance (l_a): (a) $0.01 \le l_a \le 0.05$ (b) $0.07 \le l_a \le 0.09$

Since MCRT takes into account the directly absorbed rays while the proposed method only counts the reflected rays, η_o obtained by MCRT would be larger than that obtained by the proposed method. Fig. 11 depicts the variation of the optical efficiency difference ($\Delta\eta_o$) between the MCRT's results and the proposed method's results with offset angle (a) for different offset distance (l_a). From the figure, it is clearly seen that when l_a is 0.01m, $\Delta\eta_o$ is very small (less than 0.05%), and when l_a is more than 0.03m, there is a span for a during which $\Delta\eta_o$ will reach and maintain constantly at the maximum (about 1.28%). It is easily understood that $\Delta\eta_o$ can be given by Eq. (27).

$$\Delta\eta_o = \frac{d_{re,a} \times \tau_g \times \alpha_a - l_{shade} \times \tau_g \times \alpha_a \times \rho_r \times \gamma_{shade}}{W \times \cos\theta_{in}} \times 100\% \tag{27}$$

where l_{shade} is the length of the shaded part of the reflector by absorber tube, γ_{shade} is the intercept factor for the shaded part of the reflector by absorber tube. When l_{shade} or γ_{shade} is zero, the maximum of $\Delta\eta_o$ can be obtained, which is given as follow:

$$\Delta\eta_{o,\max}=\frac{0.07\times0.96\times0.95}{5\times\cos0^{o}}\times100\%=1.28\%$$

The calculated result is completely consistent with the result shown in Fig. 11, further proving the accuracy of the proposed method. From Fig. 11, we can also observe that the larger l_a is, the larger the angle span corresponding to the maximum of $\Delta\eta_o$ will be. The possible reason is that lager l_a will be easier to cause smaller intercept factor (γ_{shade}), and hence more likely to result in the situation of $\gamma_{shade}=0$ (completely escaping of the rays reflected by the shaded area of the reflector).

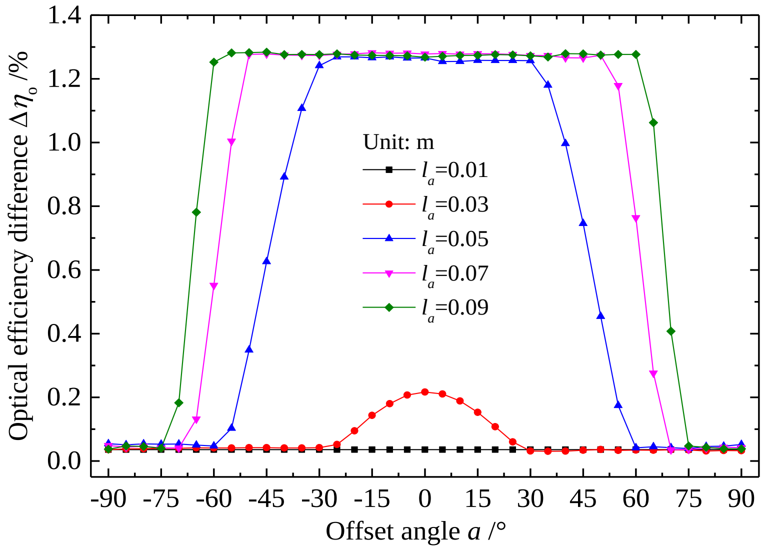

Fig. 11 Variation of optical efficiency difference ($\Delta\eta_o$) with offset angle (a) for different offset distance (l_a)

Fig. 12 shows the variation of optical efficiency (η_o) with offset distance (l_a) for different offset angle (a). We can also clearly see from the figure that the results of the proposed method are well consistent with that of MCRT, proving again the reliability and accuracy of the proposed algorithm. It is seen that η_o is kept constantly at the maximum (84.816%) for small l_a, and then drops significantly with further increasing l_a because of rays escaping effect. Fig. 13(a) shows the variations of intercept factor (γ) and optical efficiency difference ($\Delta\eta_o$) between the MCRT's results and the proposed method's results with offset distance (l_a) for different offset angle (a). It shows that γ certainly has the same variation trend as η_o. For more clarity, a partially enlarged view is shown in Fig. 13(b). It clearly displays the critical value of l_a after which η_o drops rapidly for each a. It is easily seen that the critical l_a for a=60° is the smallest (l_a=0.0228m) among the analyzed four offset angles, demonstrating that it is easiest to cause rays escaping effect for a=60°. It is known from aforementioned analyses that the offset direction that is perpendicular to the focus-edge connection line (a=68.38°) is most likely to cause rays escaping. Therefore, a=60° is the case that easiest cause rays escaping because 60° is closest to 68.38° compared to other three angles (0°, 30° and 90°). It can also be seen from Fig. 13(a) that the smaller a is, the easier $\Delta\eta_o$ reaches the maximum (1.28%), indicating that X-direction (a=0°) will be more likely to cause optical efficiency deviation from the actual value (gained by MCRT) than Y-direction does (a=90°). Fig. 14 shows the variation of critical diameter ($d_{re,a}$) with offset distance (l_a) for different offset angle (a). It can be easily seen that $d_{re,a}$ increase constantly with the increase of l_a for all a. When l_a is more than the critical value, $d_{re,a}$ will be larger than the actual tube diameter (d_a=0.07m), causing rays escaping effect and consequently leading to obvious decrease of γ (as shown in Fig.13). The critical value of l_a for each a shown in Fig. 14 is completely consistent with the result revealed in Fig. 13(b), verifying the accuracy of each other mutually.

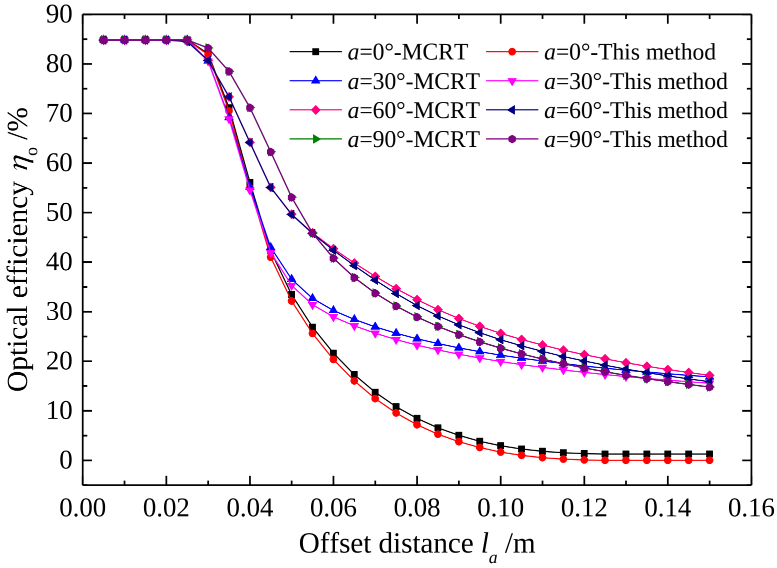

Fig. 12 Variation of optical efficiency (η_o) with offset distance (l_a) for different offset angle (a)

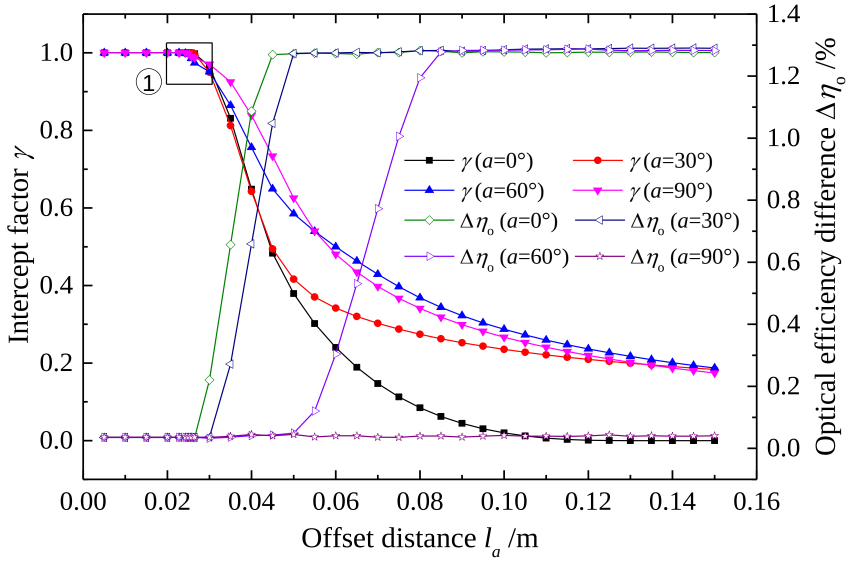

(a)

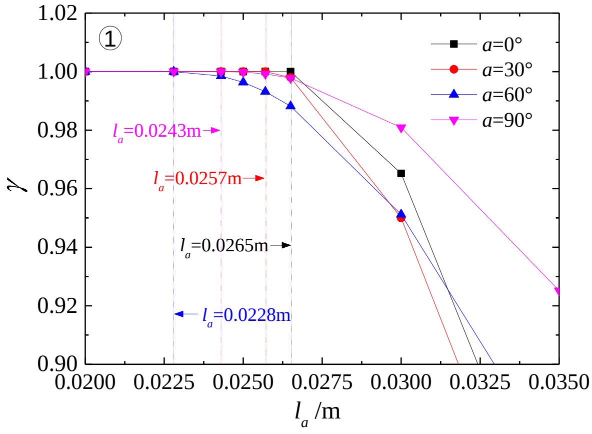

(b)

Fig. 13 Variations of intercept factor (γ) and optical efficiency difference ($\Delta\eta_o$) with offset distance (l_a) for different offset angle (a)

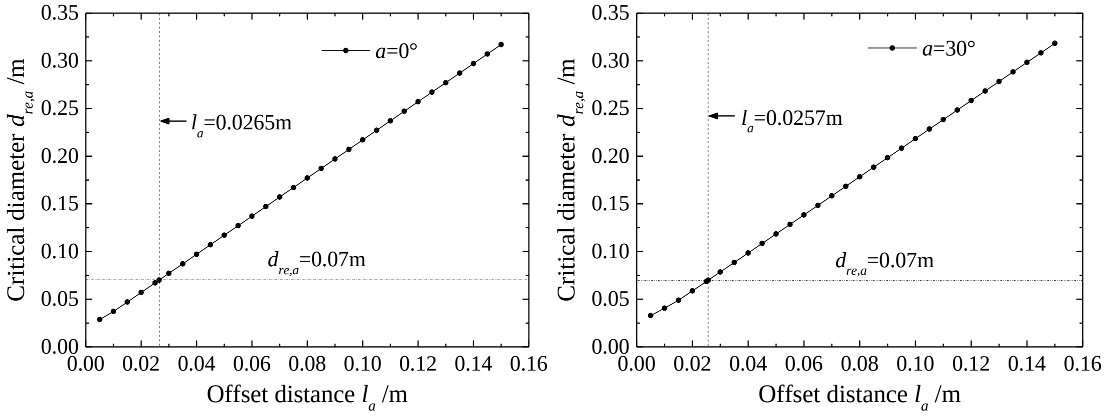

(a) (b)

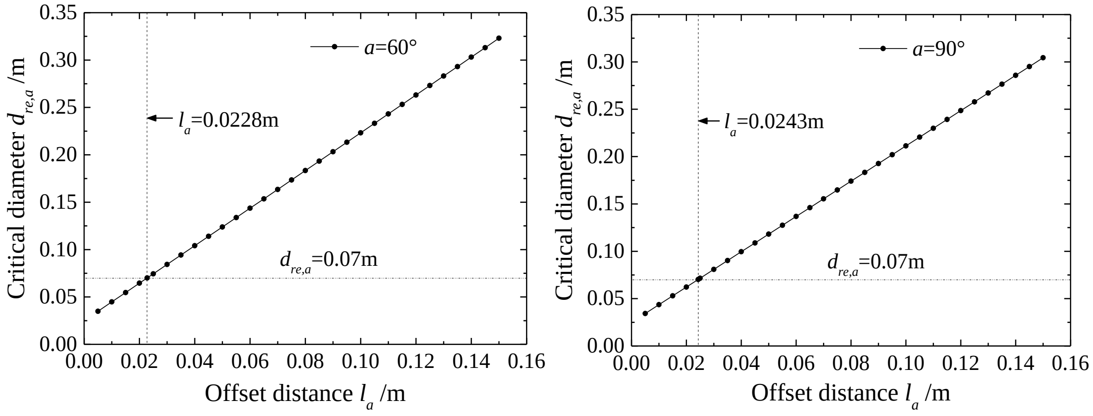

(c) (d)

Fig. 14 Variation of critical diameter ($d_{re,a}$) with offset distance (l_a) for different offset angle (a): (a) a=0°, (b) a=30°, (c) a=60°, (d) a=90°

As for MCRT, the two main influencing factors of computing time is the computer hardware, especially the CPU and RAM, and the number of used rays. In this study, a computer with the CPU of Intel Core i7-3770 (3.4 GHz) and the RAM of 8.0 GB is used for simulation. According to relevant references [30, 31], 5×10^7 rays were proved to be large enough to obtain accurate results. The greatest influencing factor of the proposed algorithm is the step size of the abscissa of point A (x_A). In this study, the step size of x_A is 0.00005 which is very small, ensuring the accuracy of the results. Taking the case that the offset angle (a) varies from -90° to 90°, the value interval of which is 5° (there are totally 37 offset angles discussed.), and the offset distance (l_a) is 0.01m as an example, we compare the required computing time of MCRT for five different numbers of rays with that of the proposed algorithm, as given in Table 3. It is clearly seen from Table 3 that the required computing time of MCRT for the discussed case is always more than 3 hours for all the discussed numbers of rays, whereas the computing time of the proposed algorithm is less than 4 seconds, indicating that the proposed algorithm has a remarkable advantage of saving time.

Table 3 Required computing time for MCRT and the proposed algorithm

Number of rays		3×10^7	4×10^7	5×10^7	6×10^7	7×10^7
Computing time	MCRT	3.29 h	4.40 h	5.48 h	6.58 h	7.69 h
	This algorithm	Less than 4 s				

Note: ‘h’ represents ‘hours’ and ‘s’ represents ‘seconds’.

3.2 Effects of structural parameters of PTC in condition of tube alignment error

Fig. 15 shows the variation of optical efficiency (η_o) with aperture width (W) for different offset angle (a) under condition of $l_a = 0.03\text{m}$. It can be clearly seen from the figure that when *a*=0° or *a*=30°, η_o is less than the maximum optical efficiency ($\eta_{o,\max}$=84.816%) for any *W*, and there exists a aperture width range in which η_o is kept constantly at 84.816% for other three offset angles (45°, 60° and 90°). The reasons are revealed in Fig. 16 which shows the variation of critical diameter ($d_{re,a}$) with aperture width (W) for different offset angle (a). It is observed that the critical diameters ($d_{re,a}$) for *a*=0° and *a*=30° are always larger than the actual tube diameter (d_a=0.07m), causing rays escaping effect and hence resulting in optical loss for all *W*. Fig. 16 also shows that when *W* is less than a certain value (critical aperture width), the critical diameters ($d_{re,a}$) for *a*=45°, *a*=60° and *a*=90° are less than 0.07m. The critical aperture widths for these three offset angles are 1.05m, 1.94m, and 3.73m respectively, which are exactly the same as the results shown in Fig. 15, proving that all the above derived formulas are accurate and reliable. From Fig. 15, we can also see that the optical efficiency (η_o) has different variation trends for different offset angles (a). This can also be well explained by the results displayed in Fig. 16. Taking *a*=30° as an example, we can give following analyses. In Fig. 16, $d_{re,a}$ increases with increasing *W* when *W* is less than 2.33m (exactly calculated by Eq. (11)), indicating that rays escaping becomes more serious with *W* increasing in this range, leading to decreasing η_o (as shown in Fig. 15). Afterwards, $d_{re,a}$ maintains constant till *W*=8.62m (exactly calculated by Eq. (12)), which demonstrates that when *W* increases from 2.33m to 8.62m, the maximum of $d_{re,a}$ just appears at *W* =2.33m. Therefore, when *W* increases from 2.33m to 8.62m, the increase rate of rays received by the absorber tube is greater than that of the rays escaping from the PTC system, consequently causing increase of η_o (as shown in Fig. 15). When *W* is more than 8.62m, $d_{re,a}$ increases consistently with the increase of *W* (as shown in Fig. 16), indicating that rays escaping becomes more serious with increasing *W*. As a result, η_o decreases constantly after *W*=8.62m (as shown in Fig. 15). It is also observed from Fig. 15 that when *W* is more than 7m, η_o decreases with the increase of *a*, which is contrary to the conclusion given in previous literature [32, 36], which stated that effects of X-direction offset (*a*=0°) was greater than that in Y-direction (*a*=90°). From Fig. 16, we can also find that when *a* is less than 90°, there is an aperture width range in which $d_{re,a}$ maintains constant, which is different from the results obtained in ideal or tracking error conditions that $d_{re,a}$ increases with increasing *W* [30-32].

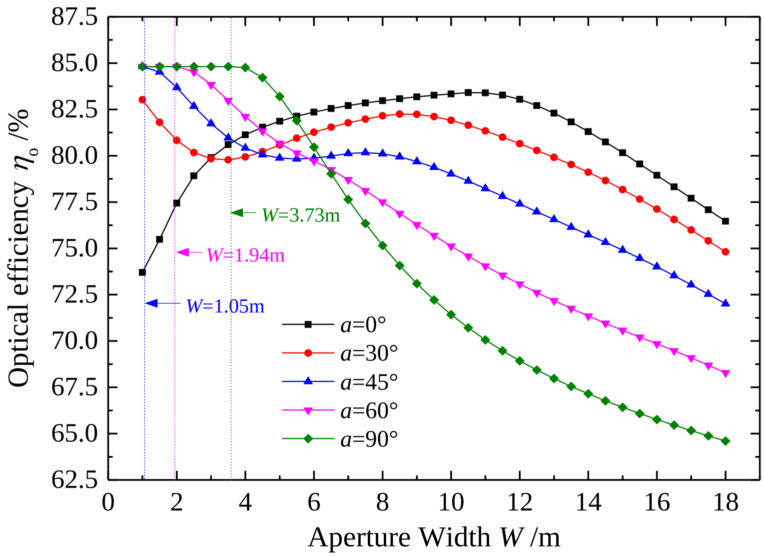

Fig. 15 Variation of optical efficiency (η_o) with aperture width (W) for different offset angle (a) ($l_a = 0.03\text{m}$)

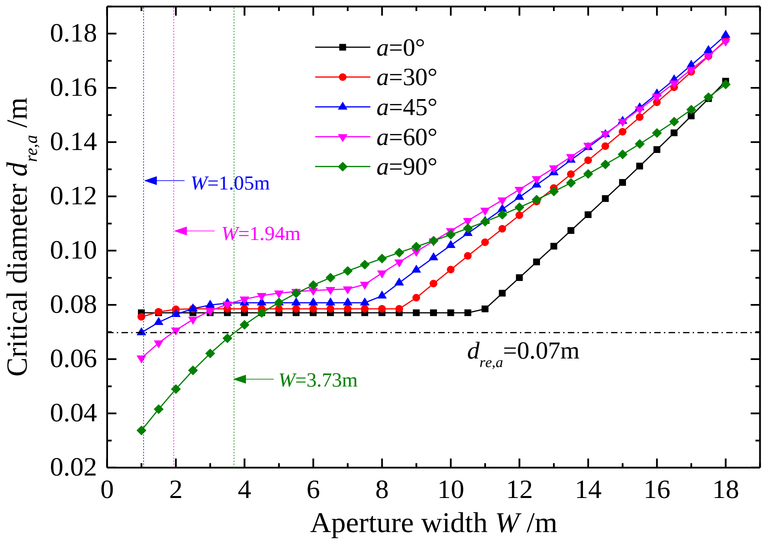

Fig. 16 Variation of critical diameter ($d_{re,a}$) with aperture width (W) for different offset angle (a) ($l_a = 0.03\text{m}$)

Fig. 17 depicts the variation of optical efficiency (η_o) with focal length (f) for different offset angle (a) under condition of $l_a = 0.03\text{m}$. It can be seen that there exists a focal length range in which η_o maintains constant at the maximum ($\eta_{o,\max}=84.816\%$) for a=0° and a=30°. Whereas, η_o for other three offset angles (45°, 60° and 90°) are always less than 84.816%. The reasons are shown in Fig. 18 which depicts the variation of critical diameter ($d_{re,a}$) with focal length (f) for different offset angle (a). From Fig. 18, it can be observed that the diameter curves for a=0° and a=30° intersect with the curve of $d_{re,a}$=0.07m, while other diameter curves do not. This demonstrates that only the cases of a=0° and a=30° have the focal length range in which the absorber tube can receive all the reflected rays, having the maximum optical efficiency. Furthermore, the critical focal length shown in Fig. 17 are completely the same as that obtained from Fig. 18, proving their accuracy mutually.

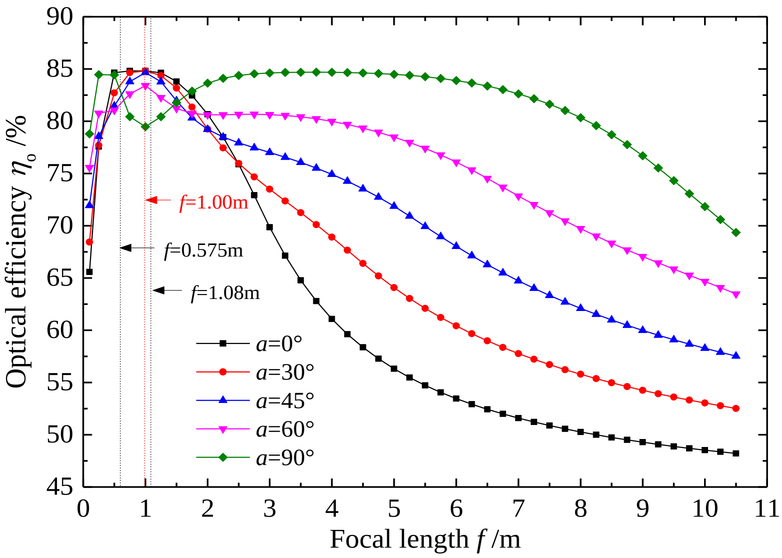

Fig. 17 Variation of optical efficiency (η_o) with focal length (f) for different offset angle (a) ($l_a=0.03$m)

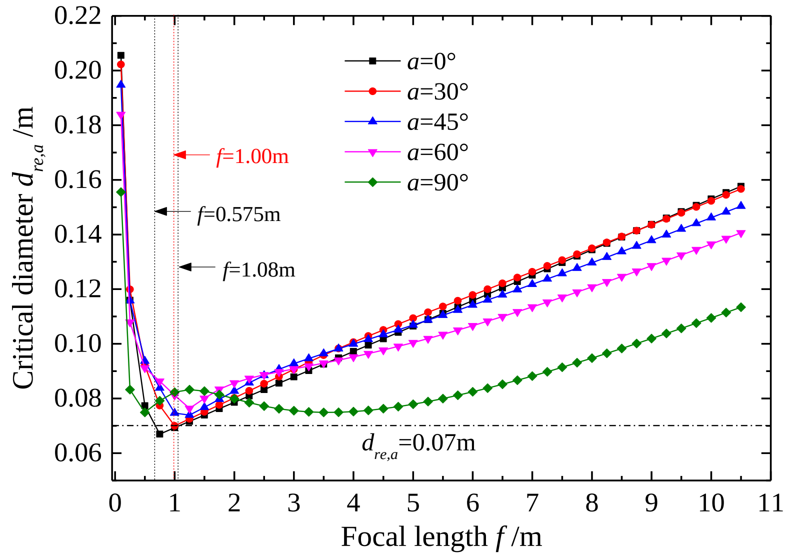

Fig. 18 Variation of critical diameter ($d_{re,a}$) with focal length (f) for different offset angle (a) ($l_a = 0.03\text{m}$)

Fig. 19 shows the variation of optical efficiency (η_o) with absorber tube diameter (d_a) for different offset angle (a) ($l_a = 0.03\text{m}$). It can be clearly seen from Fig. 19(a) that η_o first increases with the increase of d_a and then maintains constant at 84.816% with further increasing d_a. This is because the larger d_a is, the less the rays escaping from around the tube are, causing larger η_o. When d_a is more than $d_{re,a}$, η_o reaches the maximum and maintains constant. For more clarity, a partially enlarged view is shown in Fig. 19(b). It is easily seen from the figure that the critical diameter for a=60° is the largest ($d_{re,a}$=84.33mm) among the analyzed five offset angles, demonstrating that it is easiest to cause rays escaping effect for a=60°, which further verifies the above conclusion that the offset direction which is perpendicular to the focus-edge connection line (a=68.38°) is most likely to cause rays escaping. Fig. 20 shows the variation of critical diameter ($d_{re,a}$) with offset angle (a) for $l_a = 0.03\text{m}$. It is obviously seen that the critical diameters ($d_{re,a}$) for the five analyzed offset angles (0°, 30°, 45°, 60° and 90°) revealed in Fig. 20 are the same as that shown in Fig. 19. It can also be seen that the critical diameter ($d_{re,a}$) for a=68.38° is the maximum, complying very well with the conclusion that the offset direction which is perpendicular to the focus-edge connection line (a=68.38°) is most likely to cause rays escaping.

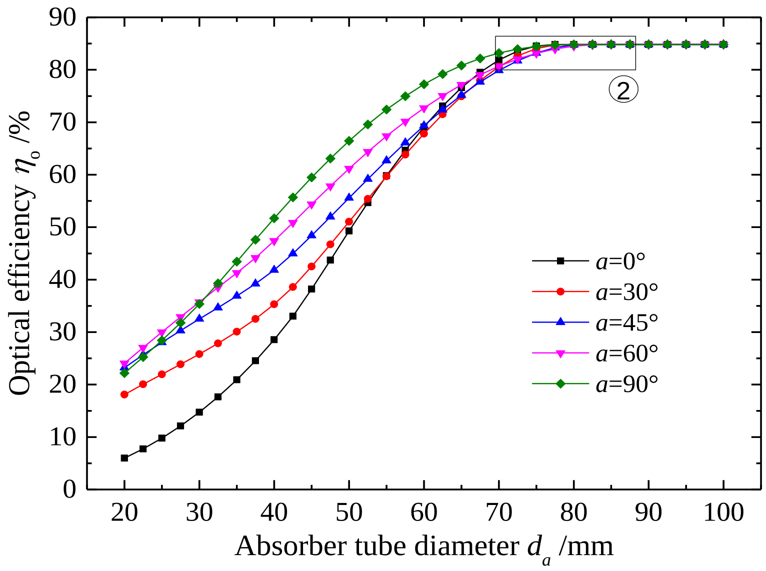

(a)

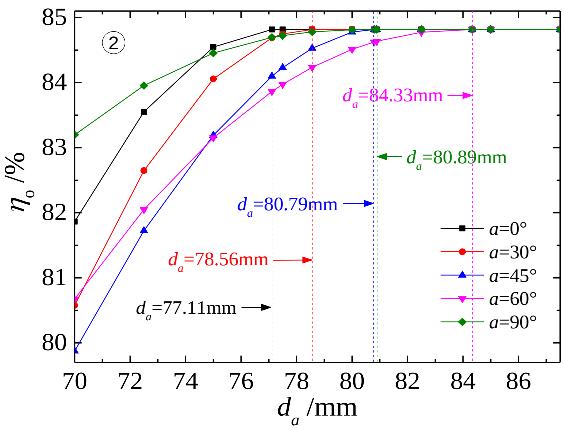

(b)

Fig. 19 Variation of optical efficiency (η_o) with absorber tube diameter (d_a) for different offset angle (a) ($l_a = 0.03\text{m}$)

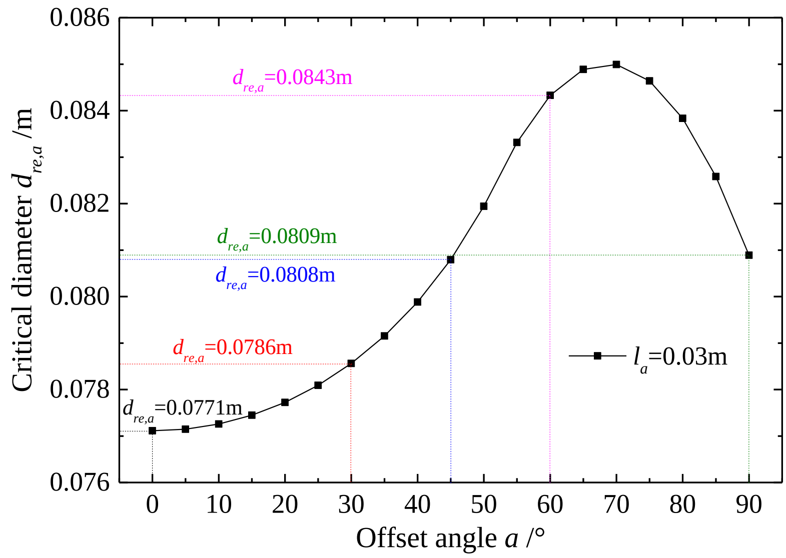

Fig. 20 Variation of critical diameter ($d_{re,a}$) with offset angle (a) for $l_a = 0.03$m

Fig. 21 shows the variation of optical efficiency (η_o) with aperture width (W) for different offset distance (l_a) under the condition of a=0°. It can be seen that η_o are always less than the maximum ($\eta_{o,\max}$ =84.816%) for l_a more than 0.03m. When l_a =0.01m or l_a =0.02m, η_o is first kept constant at 84.816% and then decreases with increasing W. The critical aperture width are 11.81m and 10.92m respectively. Fig. 22 depicts the variation of critical diameter ($d_{re,a}$) with aperture width (W) for different offset distance (l_a) under the condition of a=0°. It is clearly seen that the lager l_a is, the larger $d_{re,a}$ will be. It also shows that when l_a is more than 0.03m, $d_{re,a}$ for all W are larger than 0.07m, causing rays escaping. As for $l_a = 0.01$m and l_a =0.02m, when W is less than the critical aperture width (11.81m and 10.92m respectively), $d_{re,a}$ are smaller than 0.07m. In this case, all the reflected rays will be received by absorber tube, obtaining the maximum optical efficiency ($\eta_{o,\max}$ =84.816%). When W is more than the critical aperture width, $d_{re,a}$ will be larger than 0.07m, leading to rays escaping and hence causing optical loss.

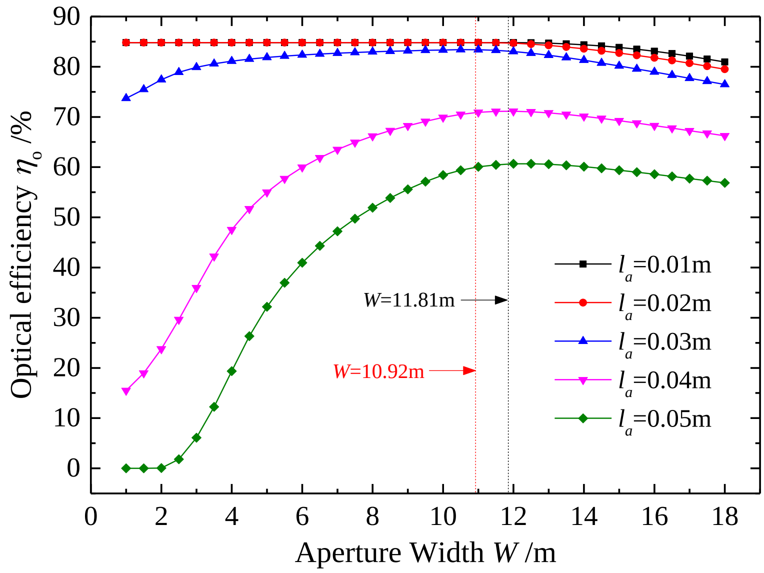

Fig. 21 Variation of optical efficiency (η_o) with aperture width (W) for different offset distance (l_a) (a=0°)

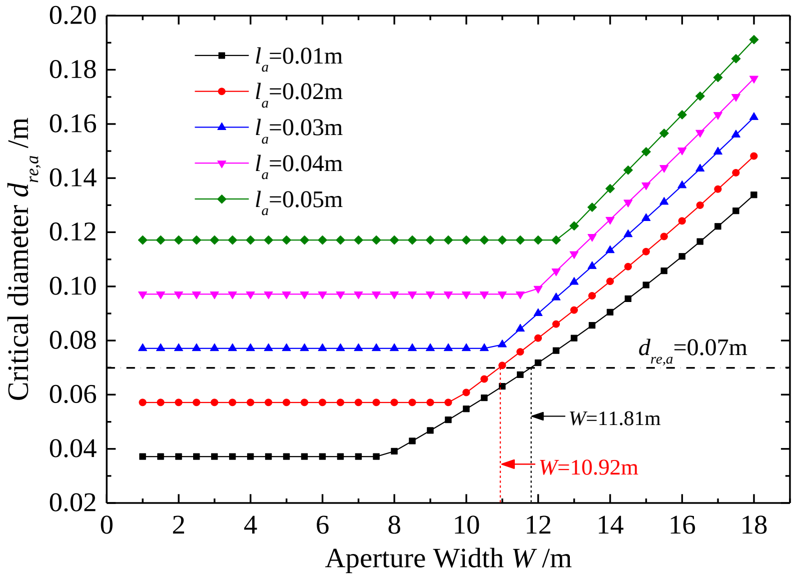

Fig. 22 Variation of critical diameter ($d_{re,a}$) with aperture width (W) for different offset distance (l_a) (a=0°)

Fig. 23 shows the variation of optical efficiency (η_o) with focal length (f) for different offset distance (l_a) under the condition of a=0°. It can be observed from the figure that when l_a is less than 0.03m, there exists a focal length range in which η_o

maintains constant at the maximum (84.816%). Whereas, η_o is consistently less than 84.816% for l_a more than 0.04m. Similarly, the reasons are shown in Fig. 24 which depicts the variation of critical diameter ($d_{re,a}$) with focal length (f) for different offset distance (l_a). From Fig. 24, we can see that the critical diameter curves for l_a =0.01m, l_a=0.02m and l_a=0.03m intersect with the curve of $d_{re,a}$=0.07m at two different points respectively, which means that there is a focal length range in which $d_{re,a}$ will be smaller than the actual tube diameter (d_a=0.07m). In this case, the absorber tube can receive all the reflected rays, ensuring the maximum of η_o.

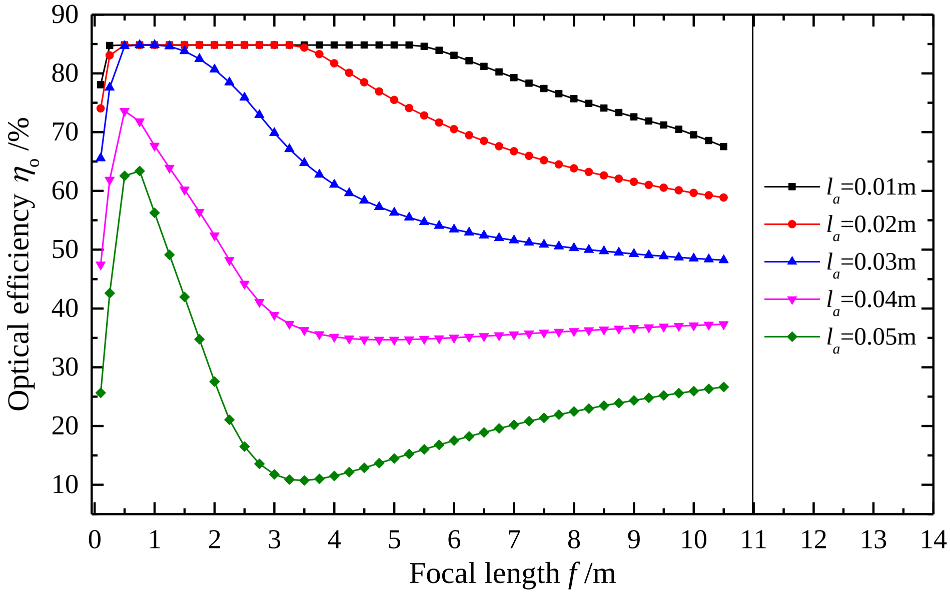

Fig. 23 Variation of optical efficiency (η_o) with focal length (f) for different offset distance (l_a) (a=0°)

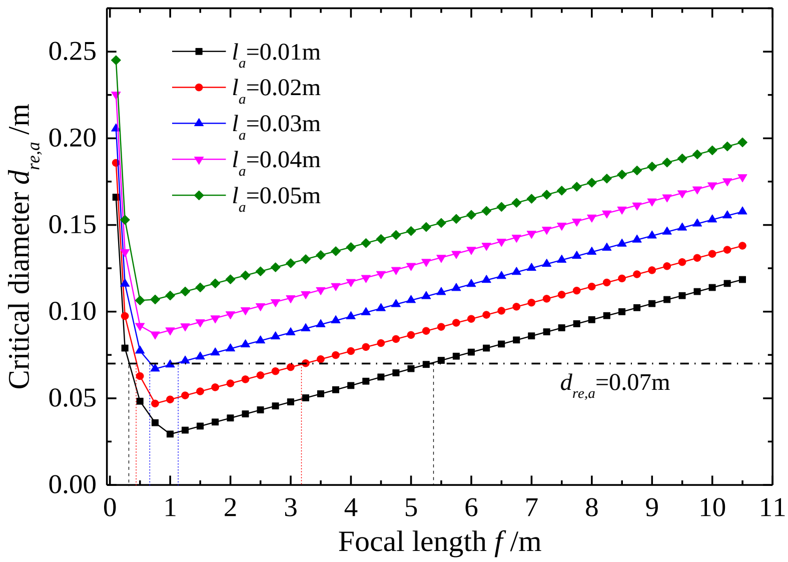

Fig. 24 Variation of critical diameter ($d_{re,a}$) with focal length (f) for different offset distance (l_a) (a=0°)

Fig. 25 shows the variation of optical efficiency (η_o) with absorber tube diameter (d_a) for different offset distance (l_a) under condition of a=0°. It is easily understood that the larger d_a is, the larger η_o will be, because of the fact that larger tube diameter can receive more reflected rays (reducing rays escaping effect). When d_a is more than the critical diameter ($d_{re,a}$), the maximum optical efficiency (84.816%) will be obtained and kept constant afterwards. Fig. 26 depicts the variation of critical diameter ($d_{re,a}$) with offset distance (l_a) for a=0°. It is clearly seen that $d_{re,a}$ increases consistently with the increase of l_a. The critical diameters ($d_{re,a}$) for the five analyzed offset distances (0.01m, 0.02m, 0.03m, 0.04m and 0.05m) revealed in Fig. 26 are completely the same as that shown in Fig. 25, proving mutually the accuracy of each other.

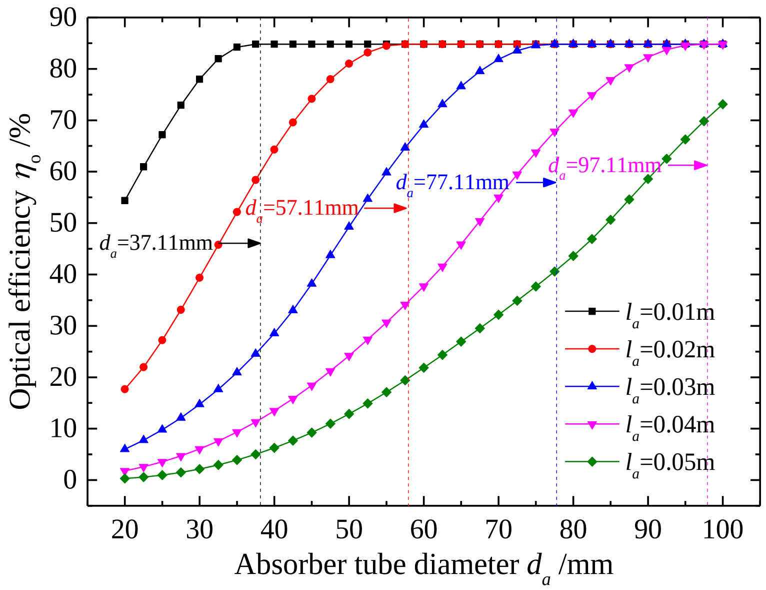

Fig. 25 Variation of optical efficiency (η_o) with absorber tube diameter (d_a) for different offset distance (l_a) (a=0°)

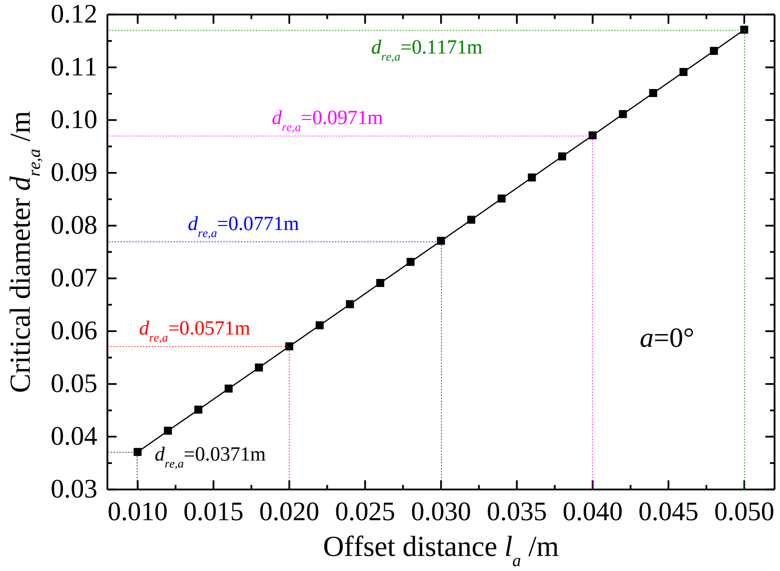

Fig. 26 Variation of critical diameter ($d_{re,a}$) with offset distance (l_a) for a=0°

4. Conclusions

In this paper, an algorithm for obtaining critical tube diameter and intercept factor (optical efficiency) of the parabolic trough solar collector (PTC) under the condition of tube alignment error is proposed. The proposed algorithm, compared with the widely used MCRT, reduces the computing time significantly from hours to seconds. The results obtained by the proposed method comply very well with that of MCRT, proving the accuracy and reliability of the proposed algorithm. The maximum optical efficiency difference between the proposed method and MCRT for LS-2 PTC module is 1.28%, which is caused by the direct insolation part. Critical tube diameters under different conditions of alignment error can be precisely calculated by using the derived formulas, which can also be used to explain very well the variation of optical efficiency (intercept factor). The proposed algorithm in this paper is the foundation of detailed geometric study which is our next work on the coupling effects of multi-errors, such as tracking error, surface error, installation error and practical sun-shape, on PTC's performance.

In addition, effects of structural parameters of the PTC (aperture width, focal length, and tube diameter) on optical performance under the condition of tube alignment error are also discussed in detail. It is revealed that the optical efficiency varies differently with structural parameters for different offset angles and offset distances. The offset direction which is perpendicular to the focus-edge connection line is not the direction that causes biggest optical loss, but the direction that is most likely to cause rays escaping. There is an aperture width (and also focal length) range in which the optical efficiency decreases with increasing offset angle, which is contrary to the conclusion presented in previous literature that effects of X-direction offset (a=0°) was greater than that in Y-direction (a=90°). Unlike the performance in ideal or tracking error conditions that the critical diameter increases with the increase of aperture width, the critical diameter maintains constant in a certain range of aperture width under the condition that the offset angle is less than 90°. The proposed method can be conveniently used to determine the allowable installation error margin of the absorber tube, and can also be used for quick calculation and analysis in engineering practice.

Acknowledgements

The authors appreciate the funding support from the research project (Grant No.: K-ZJHE) for the Joint Supervision Scheme.

References

[1] Raisul Islam M, Sumathy K, Samee UK. Solar water heating systems and their market trends. Renewable and Sustainable Energy Reviews 2013; 17: 1-25.

[2] Vijay D, Mansoor A, Soma SS, et al. Solar energy: Trends and enabling technologies. Renewable and Sustainable Energy Reviews 2013; 19: 55-564.

[3] Tian Y, Zhao CY. A review of solar collectors and thermal energy storage in solar thermal applications. Applied Energy 2013; 104: 538-553.

[4] Kalogirou SA. Solar thermal collectors and applications. Progress in Energy and Combustion Science 2004; 30: 231-295.

[5] Wang ZY, Yang WS, Qiu F, et al. Solar water heating: From theory, application, marketing and research. Renewable and Sustainable Energy Reviews 2015; 41: 68-84.

[6] Price H, Lupfert E, Kearney D, Zarza E, et al. Advances in parabolic trough solar

power technology. Journal of Solar Energy Engineering 2002; 124: 109-125.

[7] Schiel W. Collector development for solar parabolic trough power plants. Bautechnik 2012; 89: 182-191.

[8] Xu XH, Vignarooban K, Xu B, Hsu K, et al. Prospects and problems of concentrating solar power technologies for power generation in the desert regions. Renewable and Sustainable Energy Reviews 2016; 53: 1106-1131.

[9] Fernandez GA, Zarza E, Valenzuela L. Perez M. 2010. Parabolic-trough solar collectors and their applications. Renewable and Sustainable Energy Reviews 14, 1695-1721.

[10] Kalogirou SA. Parabolic trough collectors for industrial process heat in Cyprus. Energy 2002; 27: 813-830.

[11] Kalogirou SA. Use of parabolic trough solar energy collectors for sea-water desalination. Applied Energy 1998; 60: 65-88.

[12] Scrivani A, Asmar TE, Bardi U. Solar trough concentration for fresh water production and waste treatment. Desalination 2007; 206: 485-493.

[13] Bermejo P, Pino FJ, Rosa F. Solar absorption cooling plant in Seville. Solar Energy 2010; 84: 1503-1512.

[14] Cabrera FJ, Fernandez-Garcia A, Silva RMP, Perez-Garcia M. Use of parabolic trough solar collectors for solar refrigeration and air-conditioning applications. Renewable and Sustainable Energy Reviews 2013; 20: 103-118.

[15] Burkhard DG, Shealy DL, Sexl RU. Specular reflection of heat radiation from an

arbitrary reflection of heat radiation from an arbitrary receiver surface. International Journal of Heat and Mass Transfer 1973; 16: 271-280.

[16] Evans DL. On the performance of cylindrical parabolic solar concentrators with flat absorbers. Solar Energy 1977; 19: 379-385.

[17] Nicolas RO, Duran JC. Generalization of the two-dimensional optical analysis of cylindrical concentrators. Solar Energy 1980; 25: 21-31.

[18] Duran JC, Nicolas RO. Development and application of a two-dimensional optical analysis of non-perfect cylindrical concentrators. Solar Energy 1984; 34: 257-269.

[19] Jeter SM. The distribution of concentrated solar radiation in paraboloid collectors. Journal of Solar Energy Engineering 1986; 108: 219-225.

[20] Jeter SM. Calculation of the concentrated flux density distribution in parabolic trough collectors by a semifinite formulation. Solar Energy 1986; 37: 335-345.

[21] Grena R. Optical simulation of a parabolic solar trough collector. International Journal of Sustainable Energy 2010; 29: 19-36.

[22] Grena R. Efficiency Gain of a solar trough collector due to an ir-reflective film on the non-irradiated part of the receiver. International Journal of Green Energy 2011; 8: 715-733.

[23] Khanna S, Kedare SB, Singh S. Analytical expression for circumferential and axial distribution of absorbed flux on a bent absorber tube of solar parabolic trough concentrator. Solar Energy 2013; 94: 26-40.

[24] Khanna S, Sharma V, Kedare SB, Singh S. Experimental investigation of the bending of absorber tube of solar parabolic trough concentrator and comparison with analytical results. Solar Energy 2016; 125: 1-11.

[25] Wang FQ, Lin RY, Liu B, Tan HP, Shuai Y. Optical efficiency analysis of cylindrical cavity receiver with bottom surface convex. Solar Energy 2013; 90: 195-204.

[26] He YL, Xiao J, Cheng ZD, Tao YB. A MCRT and FVM coupled simulation method for energy conversion process in parabolic trough solar collector. Renewable Energy 2011; 36: 976-85.

[27] Cheng ZD, He YL, Cui FQ, Xu RJ, et al. Numerical simulation of a parabolic trough solar collector with nonuniform solar flux conditions by coupling FVM and MCRT method, Solar Energy 2012; 86: 1770-1784.

[28] Hachicha AA, Rodríguez I, Capdevila R, Oliva A. Heat transfer analysis and numerical simulation of a parabolic trough solar collector. Applied Energy 2013; 111: 581-592.

[29] Cheng ZD, He YL, Cui FQ. A new modelling method and unified code with MCRT for concentrating solar collectors and its applications. Applied Energy 2013; 101: 686-698.

[30] Cheng ZD, He YL, Wang K, Du BC, et al. A detailed parameter study on the comprehensive characteristics and performance of a parabolic trough solar collector system. Applied Thermal Engineering 2014; 63: 278-289.

[31] Cheng ZD, He YL, Cui FQ, Du BC, et al. Comparative and sensitive analysis for parabolic trough solar collectors with a detailed Monte Carlo ray-tracing optical model. Applied Energy 2014; 115: 559-572.

[32] Liang HB, You SJ, Zhang H. Comparison of three optical models and analysis of geometric parameters for parabolic trough solar collectors. Energy 2016; 96: 37-47.

[33] Guo JF, Huai XL, Liu ZG. Performance investigation of parabolic trough solar receiver. Applied Thermal Engineering 2016; 95: 357-364.

[34] Zou B, Dong JK, Yao Y, Jiang YQ. A detailed study on the optical performance of parabolic trough solar collectors with Monte Carlo Ray Tracing method based on theoretical analysis. Solar Energy 2017; 147: 189-201.

[35] Dudley V, Kolb G, Sloan M, Kearney D. SEGS LS2 solar collector–test results. Report of Sandia National Laboratories, 1994; SANDIA 94-1884, USA.

[36] Zhao DM, Xu ES, Wang ZF, Yu Q, et al. Influences of installation and tracking errors on the optical performance of a solar parabolic trough collector. Renewable Energy 2016; 94: 197-212.